Fractals

Benoit B. Mandelbrot
Michael Frame
Yale University

I. Scale Invariance
II. The Generic Notion of Fractal Dimension and a Few Specific Implementations
III. Algebra of Dimensions and Latent Dimensions
IV. Methods of Computing Dimension in Mathematical Fractals
V. Methods of Measuring Dimension in Physical Systems
VI. Lacunarity
VII. Fractal Graphs and Self-Affinity
VIII. Fractal Attractors and Repellers of Dynamical Systems
IX. Fractals and Differential or Partial Differential Equations
X. Fractals in the Arts and in Teaching

GLOSSARY

Dimension An exponent characterizing how some aspect—mass, number of boxes in a covering, etc.—of an object scales with the size of the object.
Lacunarity A measure of the distribution of hole sizes of a fractal. The prefactor in the mass–radius scaling is one such measure.
Self-affine fractal A shape consisting of smaller copies of itself, all scaled by affinities, linear transformations with different contraction ratios in different directions.
Self-similar fractal A shape consisting of smaller copies of itself, all scaled by similitudes, linear transformations with the same contraction ratios in every direction.

FRACTALS have a long history: after they became the object of intensive study in 1975, it became clear that they had been used worldwide for millenia as decorative patterns. About a century ago, their appearance in pure mathematics had two effects. It led to the development of tools like fractal dimensions, but marked a turn toward abstraction that contributed to a deep and long divide between mathematics and physics. Quite independently from fundamental mathematical physics as presently defined, fractal geometry arose in equal parts from an awareness of past mathematics and a concern for practical, mundane questions long left aside for lack of proper tools.

The mathematical input ran along the lines described by John von Neumann: "A large part of mathematics which became useful developed with absolutely no desire to be useful . . . This is true for all science. Successes were largely due to . . . relying on . . . intellectual elegance. It was by following this rule that one actually got ahead in the long run, much better than any strictly utilitarian course would have permitted . . . The principle of laissez-faire has led to strange and wonderful results."

The influence of mundane questions grew to take on far more importance than was originally expected, and recently revealed itself as illustrating a theme that is common

Encyclopedia of Physical Science and Technology, Third Edition, Volume 6

in science. Every science started as a way to organize a large collection of messages our brain receives from our senses. The difficulty is that most of these messages are very complex, and a science can take off only after it succeeds in identifying special cases that allow a workable first step. For example, acoustics did not take its first step with chirps or drums but with idealized vibrating strings. These led to sinusoids and constants or other functions invariant under translation in time. For the notion of roughness, no proper measure was available only 20 years ago. The claim put forward forcibly in Mandelbrot (1982) is that a workable entry is provided by rough shapes that are dilation invariant. These are fractals.

Fractal roughness proves to be ubiquitous in the works of nature and man. Those works of man range from mathematics and the arts to the Internet and the financial markets. Those works of nature range from the cosmos to carbon deposits in diesel engines. A sketchy list would be useless and a complete list, overwhelming. The reader is referred to Frame and Mandelbrot (2001) and to a Panorama mentioned therein, available on the web. This essay is organized around the mathematics of fractals, and concrete examples as illustrations of it.

To avoid the need to discuss the same topic twice, mathematical complexity is allowed to fluctuate up and down. The reader who encounters paragraphs of oppressive difficulty is urged to skip ahead until the difficulty becomes manageable.

I. SCALE INVARIANCE

A. On Choosing a "Symmetry" Appropriate to the Study of Roughness

The organization of experimental data into simple theoretical models is one of the central works of every science; invariances and the associated symmetries are powerful tools for uncovering these models. The most common invariances are those under Euclidean motions: translations, rotations, reflections. The corresponding ideal physics is that of uniform or uniformly accelerated motion, uniform or smoothly varying pressure and density, smooth submanifolds of Euclidean physical or phase space. The geometric alphabet is Euclidean, the analytical tool is calculus, the statistics is stationary and Gaussian.

Few aspects of nature or man match these idealizations: turbulent flows are grossly nonuniform; solid rocks are conspicuously cracked and porous; in nature and the stock market, curves are nowhere smooth. One approach to this discrepancy, successful for many problems, is to treat observed objects and processes as "roughened" versions of an underlying smooth ideal. The underlying geometry is Euclidean or locally Euclidean, and observed nature is written in the language of noisy Euclidean geometry.

Fractal geometry was invented to approach roughness in a very different way. Under magnification, smooth shapes are more and more closely approximated by their tangent spaces. The more they are magnified, the simpler ("better") they look. Over some range of magnifications, looking more closely at a rock or a coastline does not reveal a simpler picture, but rather more of the same kind of detail. Fractal geometry is based on this ubiquitous *scale invariance*. "A fractal is an object that doesn't look any better when you blow it up." Scale invariance is also called "symmetry under magnification."

A manifestation is that fractals are sets (or measures) that can be broken up into pieces, each of which closely resembles the whole, except it is smaller. If the pieces scale isotropically, the shape is called *self-similar*; if different scalings are used in different directions, the shape is called *self-affine*.

There are deep relations between the geometry of fractal sets and the renormalization approach to critical phenomena in statistical physics.

B. Examples of Self-Similar Fractals

1. Exact Linear Self-Similarity

A shape S is called *exactly (linearly) self-similar* if the whole S splits into the union of parts S_i: $S = S_1 \cup S_2 \cup \ldots \cup S_n$. The parts satisfy two restrictions: (a) each part S_i is a copy of the whole S scaled by a linear contraction factor r_i, and (b) the intersections between parts are empty or "small" in the sense of dimension. Anticipating Section II, if $i \neq j$, the fractal dimension of the intersection $S_i \cap S_j$ must be lower than that of S. The roughness of these sets is characterized by the *similarity dimension* d. In the special equiscaling case $r_1 = \cdots = r_n = r$, $d = \log(n)/\log(1/r)$. In general, d is the solution of the *Moran equation*

$$\sum_{i=1}^{n} r_i^d = 1.$$

More details are given in Section II.

Exactly self-similar fractals can be constructed by several elegant mathematical approaches.

a. Initiator and generator. An *initiator* is a starting shape; a *generator* is a juxtaposition of scaled copies of the initiator. Replacing the smaller copies of the initiator in the generator with scaled copies of the generator sets in motion a process whose limit is an exactly self-similar fractal. Stages before reaching the limit are called *protofractals*. Each copy is anchored by a fixed point, and one may have to specify the orientation of each replacement. The

FIGURE 1 Construction of the Sierpinksi gasket. The initiator is a filled-in equilateral triangle, and the generator (on the left) is made of $N = 3$ triangles, each obtained from the initiator by a contraction map T_i of reduction ratio $r = 1/2$. The contractions' fixed points are the vertices of the initiator. The middle shows the second stage, replacing each copy of the initiator with a scaled copy of the generator. On the right is the seventh stage of the construction.

Sierpinski gasket (Fig. 1) is an example. The eye spontaneously splits the whole S into parts. The simplest split yields $N = 3$ parts S_i, each a copy of the whole reduced by a similitude of ratio $1/2$ and with fixed point at a vertex of the initiator. In finer subdivisions, $S_i \cap S_j$ is either empty or a single point, for which $d = 0$. In this example, but not always, it can be made empty by simply erasing the topmost point of every triangle in the construction.

Some of the most familiar fractals were orignally constructed to provide instances of curves that exemplify properties deemed counterintuitive: classical curves may have one multiple point (like Fig. 8) or a few. To the contrary, the Sierpinski gasket (Fig. 2, far left) is a curve with dense multiple points. The Sierpinski carpet (Fig. 2, mid left) is a universal curve in the sense that one can embed in the carpet every plane curve, irrespective of the collection of its multiple points. The Peano curve [initiator the diagonal segment from (0, 0) to (1, 1), generator in Fig. 2 mid right] is actually not a curve but a motion. It is plane-filling: a continuous onto map $[0, 1] \to [0, 1] \times [0, 1]$.

b. Iterated function systems. Iterated function systems (IFS) are a formalism for generating exactly self-similar fractals based on work of Hutchinson (1981) and Mandelbrot (1982), and popularized by Barnsley (1988). IFS are the foundation of a substantial industry of image compression. The basis is a (usually) finite collection $\{T_1, \ldots, T_n\}$ of contraction maps $T_i: \mathbf{R}^n \to \mathbf{R}^n$ with contraction ratios $r_i < 1$. Each T_i is assigned a probability p_i that serves, at each (discrete) instant of time, to select the next map to be used. An IFS attractor also can be viewed as the limit set of the orbit $\mathcal{O}^+(x_0)$ of any point x_0 under the action of the semigroup generated by $\{T_1, \ldots, T_n\}$.

The formal definition of IFS, which is delicate and technical, proceeds as follows. Denoting by $\mathcal{K}$ the set of nonempty compact subsets of $\mathbf{R}^n$ and by h the Hausdorff metric on $\mathcal{K}$ [$h(A, B) = \inf\{\delta: A \subset B_\delta \text{ and } B \subset A_\delta\}$, where $A_\delta = \{x \in \mathbf{R}^n: d(x, y) \le \delta \text{ for some } y \in A\}$ is the δ-*thickening* of A, and d is the Euclidean metric], the T_i together define a transformation $\mathcal{T}: \mathcal{K} \to \mathcal{K}$ by $\mathcal{T}(A) = \bigcup_{i=1}^{n} \{T_i(x): x \in A\}$, a contraction in the Hausdorff metric with contraction ratio $r = \max\{r_1, \ldots, r_n\}$. Because $(\mathcal{K}, h)$ is complete, the contraction mapping principle guarantees there is a unique fixed point C of $\mathcal{T}$. This fixed point is the *attractor* of the IFS $\{T_1, \ldots, T_n\}$. Moreover, for any $K \in \mathcal{K}$, the sequence $K, \mathcal{T}(K), \mathcal{T}^2(K), \ldots$ converges to C in the sense that $\lim_{n \to \infty} h(\mathcal{T}^n(K), C) = 0$.

The IFS *inverse problem* is, for a given compact set A and given tolerance $\delta > 0$, to find a set of transformations $\{T_1, \ldots, T_n\}$ with attractor C satisfying $h(A, C) < \delta$. The search for efficient algorithms to solve the inverse problem is the heart of *fractal image compression*. Detailed discussions can be found in Barnsley and Hurd (1993) and Fischer (1995).

2. Exact Nonlinear Self-Similarity

A broader class of fractals is produced if the decomposition of S into the union $S = S_1 \cup S_2 \cup \ldots \cup S_n$ allows the S_i to be the images of S under nonlinear transformations.

a. Quadratic Julia sets. For fixed complex number c, the "quadratic orbit" of the starting complex number z is a sequence of numbers that begins with $f_c(z) = z^2 + c$, then $f_c^2(z) = (f_c(z))^2 + c$ and continues by following the rule $f_c^n(z) = f_c(f_c^{n-1}(z))$. The *filled-in (quadratic) Julia set* consists of the starting points that do not iterate to infinity, formally, the points $\{z: f_c^n(z)$ remains bounded as $n \to \infty\}$. The *(quadratic) Julia set* J_c is the boundary of the filled-in Julia set. Figure 3 shows the Julia set J_c for $c = 0.4 + 0 \cdot i$ and the filled-in Julia set for $c = -0.544 + 0.576 \cdot i$. The latter has an attracting 5-cycle, the black region is the basin of attraction of the

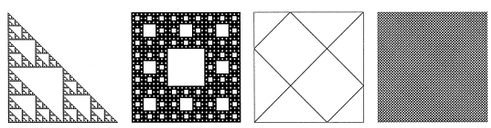

FIGURE 2 The Sierpinski gasket, Sierpinski carpet, the Peano curve generator, and the fourth stage of the Peano curve.

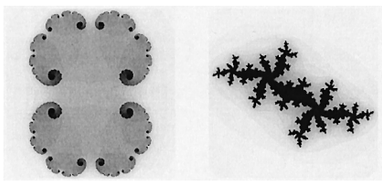

FIGURE 3 The Julia set of $z^2 + 0.4$ (left) and the filled-in Julia set for $z^2 - 0.544 + 0.576 \cdot i$ (right).

5-cycle, and the Julia set is the boundary of the black region. Certainly, J_c is invariant under f_c and under the inverses of f_c, $f_{c+}^{-1}(z) = \sqrt{z-c}$ and $f_{c-}^{-1}(z) = -\sqrt{z-c}$. Polynomial functions allow several equivalent characterizations: J_c is the closure of the set of repelling periodic points of $f_c(z)$ and J_c is the attractor of the nonlinear IFS $\{f_{c+}^{-1}, f_{c-}^{-1}\}$.

Much is known about Julia sets of quadratic functions. For example, McMullen proved that at a point whose rotation number has periodic continued-fraction expansion, the J set is asymptotically self-similar about the critical point.

The J sets are defined for functions more general than polynomials. Visually striking and technically interesting examples correspond to the Newton function $N_f(z) = z - f(z)/f'(z)$ for polynomial families $f(z)$, or entire functions like $\lambda \sin z$, $\lambda \cos z$, or $\lambda \exp z$ (see Section VIII.B). Discussions can be found in Blanchard (1994), Curry *et al.* (1983), Devaney (1994), Keen (1994), and Peitgen (1989).

b. The Mandelbrot set. The quadratic orbit $f_c^n(z)$ always converges to infinity for large enough values of z. Mandelbrot attempted a computer study of the set M^0 of those values of c for which the orbit does *not* converge to infinity, but to a stable cycle. This approach having proved unrewarding, he moved on to a set that promised an easier calculation and proved spectacular. Julia and Fatou, building on fundamental work of Montel, had shown that the Julia set J_c of $f_c(z) = z^2 + c$ must be either connected or totally disconnected. Moreover, J_c is connected if, and only if, the orbit $\mathcal{O}^+(0)$ of the critical point $z = 0$ remains bounded. The set M defined by $\{c\colon f_c^n(0)$ remains bounded$\}$ is now called the *Mandelbrot set* (see the left side of Fig. 4). Mandelbrot (1980) performed a computer investigation of its structure and reported several observations. As is now well known, small copies of the M set are infinitely numerous and dense in its boundary. The right side of Fig. 4 shows one such small copy, a nonlinearly distorted copy of the whole set. Although the small copy on the right side of Fig. 4 appears to be an isolated "island," Mandelbrot conjectured and Douady and Hubbard (1984) proved that the M set is connected. Sharpening an observation by Mandelbrot, Tan Lei (1984) proved the convergence of appropriate magnifications of Julia sets and the M set at certain points named after Misiurewicz. Shishikura (1994) proved Mandelbrot's (1985) and Milnor's (1989) conjecture that the boundary of the M set has Hausdorff dimension 2. Lyubich proved that the boundary of the M set is asymptotically self-similar about the Feigenbaum point.

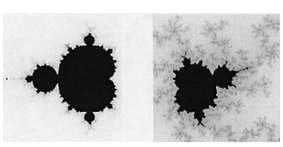

FIGURE 4 Left: The Mandelbrot set. Right: A detail of the Mandelbrot set showing a small copy of the whole. Note the nonlinear relation between the whole and the copy.

Mandelbrot's first conjecture, that the interior of the M set consists entirely of components (called *hyperbolic*) for which there is a stable cycle, remains unproved in general, though McMullen (1994) proved it for all such components that intersect the real axis. Mandelbrot's notion that M may be the closure of M^0 is equivalent to the assertion that the M set is locally connected. Despite intense efforts, that assertion remains a conjecture, though Yoccoz and others have made progress.

Other developments include the theory of quadratic-like maps (Douady and Hubbard, 1985), implying the universality and ubiquity of the M set. This result was presaged by the discovery (Curry *et al.*, 1983) of a Mandelbrot set in the parameter space of Newton's method for a family of cubic polynomials.

The recent book by Tan Lei (2000) surveys current results and attests to the vitality of this field.

c. Circle inversion limit sets. Inversion I_C in a circle C with center O and radius r transforms a point P into the point P' lying on the ray OP and with $d(O, P) \cdot d(O, P') = r^2$. This is the orientation-reversing involution defined on $\mathbf{R}^2 \cup \{\infty\}$ by $P \to I_C(P) = P'$. Inversion in C leaves C fixed, and interchanges the interior and exterior of C. It contracts the "outer" component not containing O, but the contraction ratio is not bounded by any $r < 1$.

Poincaré generalized from inversion in one circle to a collection of more than one inversion. As an example, consider a collection of circles $C_1, \ldots, C_N$ each of which is external to all the others. That is, for all $j \neq i$, the disks bounded by C_i and C_j have disjoint interiors. The *limit set* $\Lambda(C_1, \ldots, C_N)$ of inversion in these circles is the set of limit points of the orbit $\mathcal{O}^+(P)$ of any point P, external to $C_1, \ldots, C_N$, under the group generated by $I_{C_1}, \ldots, I_{C_N}$. Equivalently, it is the set left invariant by every one of the inversions $I_{C_1}, \ldots, I_{C_N}$.

The limit set Λ is nearly always fractal but the nonlinearity of inversion guarantees that Λ is nonlinearly self-similar. An example is shown in Fig. 5: the part of the limit set inside C_1 is easily seen to be the transform by I_1 of the part of the limit set inside C_2, C_3, C_4, and C_5.

How can one draw the limit set Λ when the arrangement of the circles $C_1, \ldots, C_N$ is more involved? Poincaré's original algorithm converges extraordinarily slowly. The first alternative algorithm was advanced in Mandelbrot

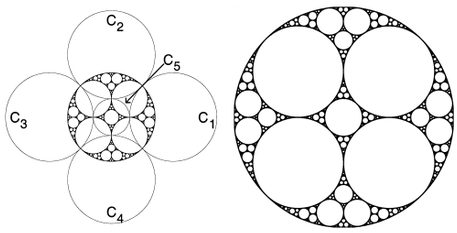

FIGURE 5 Left: The limit set generated by inversion in the five circles $C_1, \ldots, C_5$. Right: A magnification of the limit set.

(1982, Chapter 18); it is intuitive and the large-scale features of Λ appear very rapidly, followed by increasingly fine features down to any level a computer's memory can support.

d. Kleinian group limit sets. A Kleinian group (Beardon, 1983; Maskit, 1988) is a discrete group of Möbius transformations

$$z \to \frac{az+b}{cz+d}$$

acting on the Riemann sphere $\hat{\mathbf{C}}$, the sphere at infinity of hyperbolic 3-space $\mathbf{H}^3$. The isometries of $\mathbf{H}^3$ can be represented by complex matrices

$$\begin{bmatrix} a & b \\ c & d \end{bmatrix}.$$

[More precisely, by their equivalence classes in $PSL_2(\mathbf{C})$.] Sullivan's side-by-side dictionary (Sullivan, 1985) between Kleinian groups and iterates of rational maps is another deep mathematical realm informed, at least in part, by fractal geometry. Thurston's "geometrization program" for 3-manifolds (Thurston, 1997) involves giving many 3-manifolds hyperbolic structures by viewing them as quotients of $\mathbf{H}^3$ by the action of a Kleinian group G (Epstein, 1986). The corresponding action of G on $\hat{\mathbf{C}}$ determines the limit set $\Lambda(G)$, defined as the intersection of all nonempty G-invariant subsets of $\hat{\mathbf{C}}$. For many G, the limit set is a fractal. An example gives the flavor of typical results: the limit set of a finitely generated Kleinian group is either totally disconnected, a circle, or has Hausdorff dimension greater than 1 (Bishop and Jones, 1997). The Hausdorff dimension of the limit set has been studied by Beardon, Bishop, Bowen, Canary, Jones, Keen, Mantica, Maskit, McMullen, Mumford, Parker, Patterson, Sullivan, Tricot, Tukia, and many others. Poincaré exponents, eigenvalues of the Laplacian, and entropy of geodesic flows are among the tools used.

Figure 5 brings forth a relation between some limit sets of inversions or Kleinian groups and Apollonian packings (Keen *et al.*, 1993). In fact, the limit set of the Kleinian groups that are in the Maskit embedding (Keen and Series, 1993) of the Teichmüller space of any finite-type Riemann surface are Apollonian packings. These correspond to hyperbolic 3-manifolds having totally geodesic boundaries. McShane *et al.* (1994) used automatic group theory to produce efficient pictures of these limit sets, and Parker (1995) showed that in many cases the Hausdorff dimension of the limit set equals the circle packing exponent, easily estimated as the slope of the log–log plot of the number of circles of radius $\geq r$ (y axis) versus r (x axis).

Limit sets of Kleinian group actions are an excellent example of a deep, subtle, and very active area of pure mathematics in which fractals play a central role.

3. Statistical Self-Similarity

A tree's branches are not exact shrunken copies of that tree, inlets in a bay are not exact shrunken copies of that bay, nor is each cloud made up of exact smaller copies of that cloud. To justify the role of fractal geometry as a geometry of nature, one must take a step beyond exact self-similarity (linear or otherwise). Some element of randomness appears to be present in many natural objects and processes. To accommodate this, the notions of self-similarity and self-affinity are made statistical.

a. Wiener brownian motion: its graphs and trails. The first example is classical. It is one-dimensional Brownian motion, the random process $X(t)$ defined by these properties: (1) with probability 1, $X(0) = 0$ and $X(t)$ is continuous, and (2) the increments $X(t+\Delta t) - X(t)$ of $X(t)$ are Gaussian with mean 0 and variance Δt. That is,

$$Pr\{X(t+\Delta t) - X(t) \leq x\} = \frac{1}{\sqrt{2\pi\,\Delta t}} \times \int_{-\infty}^{x} \exp\left(\frac{-u^2}{2\Delta t}\right) du.$$

An immediate consequence is independence of increments over disjoint intervals. A fundamental property of Brownian motion is statistical self-affinity: for all $s > 0$,

$$Pr\{X(s(t+\Delta t)) - X(st) \leq \sqrt{s}x\} = Pr\{X(t+\Delta t) - X(t) \leq x\}.$$

That is, rescaling t by a factor of s, and of x by a factor of $\sqrt{s}$, leaves the distribution unchanged. This correct rescaling is shown on the left panel of Fig. 6: t (on the horizontal axis) is scaled by 4, x (on the vertical axis) is scaled by $2 = 4^{1/2}$. Note that this magnification has about the same degree of roughness as the full picture. In the center panel, t is scaled by 4, x by 4/3; the magnification is flatter than the original. In the right panel, both t and

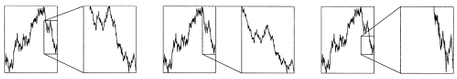

FIGURE 6 Left panel: Correct rescaling illustrating the self-affinity of Brownian motion. Center and right panels: Two incorrect rescalings.

x are scaled by 4; the magnification is steeper than the original.

A sequence of increments of Brownian motion is called Gaussian white noise. Even casual inspection of the graph reveals some fundamental features. The width of an old pen-plotter line being equal to the spacing between successive difference values, the bulk of the difference plot merges into a "band" with the following properties (see Fig. 7):

- The band's width is approximately constant.
- The values beyond that band stay close to it (this is due to the fact that the Gaussian has "short tails").
- The values beyond that band do not cluster.

Positioning E independent one-dimensional Brownian motions along E coordinate axes gives a higher dimensional Brownian motion: $B(t) = \{X_1(t), \ldots, X_E(t)\}$. Plotted as a curve in E-dimensional space, the collection of points that $B(t)$ visits between $t = 0$ and $t = 1$ defines a *Brownian trail*.

When $E > 2$, this is an example of a statistically self-similar fractal. To split the Brownian trail into N reduced-scale parts, pick $N - 1$ arbitrary instants t_n with $0 = t_0 < t_1 < \cdots < t_{N-1} < t_N = 1$. The Brownian trail for $0 \le t \le 1$ splits into N subtrails B_n for the interval $t_{n-1} < t < t_n$. The parts B_n follow the same statistical distribution as the whole, after the size is expanded by $(t_n - t_{n-1})^{-1/2}$ in every direction.

Due to the definition of self-similarity, this example reveals a pesky complication: for $i \neq j$, $B_i \cap B_j$ must be of dimension less than B. This is indeed the case if $E > 2$, but not in the plane $E = 2$. However, the overall idea can be illustrated for $E = 2$. The right side of Fig. 8 shows $B_1(t)$ for $0 \le t \le 1/4$, expanded by a factor of $2 = (1/4 - 0)^{-1/2}$ and with additional points interpolated so the part and the whole exhibit about the same number of turns. The details for $E = 2$ are unexpectedly complex, as shown in Mandelbrot (2001b, Chapter 3).

The dimensions (see Sections II.B and II.E) of some Brownian constructions are well-known, at least in most cases. For example, with probability 1:

FIGURE 7 Plot of 4000 successive Brownian increments.

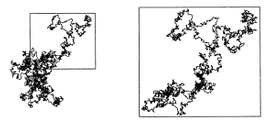

FIGURE 8 A Brownian trail. Right: The first quarter of the left trail, magnified and with additional turns interpolated so the left and right pictures have about the same number of turns.

- For $E \ge 2$ a Brownian trail $B: [0, 1] \to \mathbf{R}^E$ has Hausdorff and box dimensions $d_{\mathrm{H}} = d_{\mathrm{box}} = 2$, respectively.
- The graph of one-dimensional Brownian motion $B: [0, 1] \to \mathbf{R}$ has $d_{\mathrm{H}} = d_{\mathrm{box}} = 3/2$.

Some related constructions have been more resistant to theoretical analysis. Mandelbrot's *planar Brownian cluster* is the graph of the complex $B(t)$ constrained to satisfy $B(0) = B(1)$. It can be constructed by linearly detrending the x- and y-coordinate functions: $(X(t) - tX(1), Y(t) - tY(1))$. See Fig. 9. The cluster is known to have dimension 2. Visual inspection supported by computer experiments led to the $4/3$ *conjecture*, which asserts that the boundary of the cluster has dimension $4/3$ (Mandelbrot, 1982, p. 243). This has been proved by Lawler *et al.* (2000).

Brownian motion is the unique stationary random process with increments independent over disjoint intervals and with finite variance. For many applications, these conditions are too restrictive, drawing attention to other random processes that retain scaling but abandon either independent increments or finite variance.

b. Fractional Brownian motion. For fixed $0 < H < 1$, *fractional Brownian motion* (FBM) of exponent H is a random process $X(t)$ with increments $X(t + \Delta t) - X(t)$ following the Gaussian distribution with mean 0 and standard deviation $(\Delta t)^H$. Statistical self-affinity is straightforward: for all $s > 0$

$$Pr\{X(s(t + \Delta t)) - X(st) \le s^H x\}$$
$$= Pr\{X(t + \Delta t) - X(t) \le x\}.$$

The correlation is the expected value of the product of successive increments. It equals

FIGURE 9 A Brownian cluster.

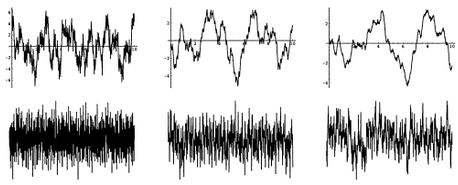

FIGURE 10 Top: Fractional Brownian motion simulations with $H = 0.25$, $H = 0.5$, and $H = 0.75$. Bottom: Difference plots $X(t + 1) - X(t)$ of the graphs above.

$$E((X(t) - X(0)) \cdot (X(t + h) - X(t))) = \tfrac{1}{2}((t + h)^{2H} - t^{2H} - h^{2H}).$$

If $H = 1/2$, this correlation vanishes and the increments are independent. In fact, FBM reduces to Brownian motion. If $H > 1/2$, the correlation is positive, so the increments tend to have the same sign. This is *persistent FBM*. If $H < 1/2$, the correlation is negative, so the increments tend to have opposite signs. This is *antipersistent FBM*. See Fig. 10. The exponent determines the dimension of the graph of FBM: with probability 1, $d_{\mathrm{H}} = d_{\mathrm{box}} = 2 - H$. Notice that for $H > 1/2$, the central band of the difference plot moves up and down, a sign of long-range correlation, but the outliers still are small. Figure 11 shows the trails of these three flavors of FBM. FBM is the main topic of Mandelbrot (2001c).

c. Lévy stable processes. While FBM introduces correlations, its increments remain Gaussian and so have small outliers. The Gaussian distribution is characterized by its first two moments (mean and variance), but some natural phenomena appear to have distributions for which these are not useful indicators. For example, at the critical point of percolation there are clusters of all sizes and the expected cluster size diverges.

Paul Lévy studied random walks for which the jump distributions follow the power law $Pr\{X > x\} \approx x^{-\alpha}$. There is a geometrical approach for generating examples of Lévy processes.

The *unit step function* $\xi(t)$ is defined by

$$\xi(t) = \begin{cases} 0 & \text{for } x < 0 \\ 1 & \text{for } x \geq 0 \end{cases}$$

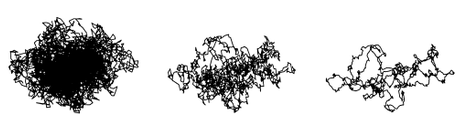

FIGURE 11 Top: Fractional Brownian motion simulations with $H = 0.25$, $H = 0.5$, and $H = 0.75$. Bottom: Difference plots $X(t + 1) - X(t)$ of the graphs above.

FIGURE 12 Lévy flight on the line. Left: the graph as a function of time. Right, the increments.

and a (one-dimensional) Lévy stable process is defined as a sum

$$f(t) = \sum_{k=1}^{\infty} \lambda_k \xi(t - t_k),$$

where the pulse times t_n and amplitudes λ_n are chosen according to the following Lévy measure: given t and λ, the probability of choosing (t_i, λ_i) in the rectangle $t < t_i < t + dt$, $\lambda < \lambda_i < \lambda + d\lambda$ is $C\lambda^{-\alpha - 1}\, d\lambda\, dt$. Figure 12 shows the graph of a Lévy process or flight, and a graph of its increments.

Comparing Figs. 7, 10, and 12 illustrates the power of the increment plot for revealing both global correlations (FBM) and long tails (Lévy processes).

The effect of large excursions in Lévy processess is more visible in the plane. See Fig. 13. These Lévy flights were used in Mandelbrot (1982, Chapter 32) to mimic the statistical properties of galaxy distributions.

Using fractional Brownian motion and Lévy processes, Mandelbrot (in 1965 and 1963) improved upon Bachelier's Brownian model of the stock market. The former corrects the independence of Brownian motion, the latter corrects its short tails. The original and corrected processes in the preceding sentence are statistically self-affine random fractal processes. This demonstrates the power of invariances in financial modeling; see Mandelbrot (1997a,b).

d. Self-affine cartoons with mild to wild randomness. Many natural processes exhibit long tails or global dependence or both, so it was a pleasant surprise that both can be incorporated in an elegant family of simple cartoons. (Mandelbrot, 1997a, Chapter 6; 1999, Chapter N1; 2001a). Like for self-similar curves (Section I.B.1.a), the basic construction of the cartoon involves an initiator and a

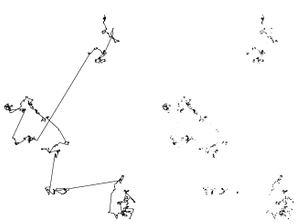

FIGURE 13 Left: Trail of the Lévy flight in the plane. Right: The Lévy dust formed by the turning points.

FIGURE 14 The initiator (left), generator (middle), and first generation (right) of the Brownian cartoon.

generator. The process used to generate the graph consists in replacing each copy of the initiator with an appropriately rescaled copy of the generator. For a Brownian cartoon, the initiator can be the diagonal of the unit square, and the generator, the broken line with vertices (0, 0), (4/9, 2/3), (5/9, 1/3), and (1, 1). Pictured in Fig. 14 are the initiator (left), generator (middle), and first iteration of the process (right).

To get an appreciation for how quickly the local roughness of these pictures increases, the left side of Fig. 15 shows the sixth iterate of the process.

Self-affinity is built in because each piece is an appropriately scaled version of the whole. In Fig. 14, the scaling ratios have been selected to match the "square root" property of Brownian motion: for each segment of the generator we have $|\Delta x_i| = (\Delta t_i)^{1/2}$.

More generally, a cartoon is called *unifractal* if there is a constant H with $|\Delta x_i| = (\Delta t_i)^H$ for each generator segment, where $0 < H < 1$. If different H are needed for different segments, the cartoon is *multifractal*.

The left side of Figure 15 is too symmetric to mimic any real data, but this problem is palliated by shuffling the order in which the three pieces of the generator are put into each scaled copy. The right side of Fig. 15 shows a Brownian cartoon randomized in this way.

Figure 16 illustrates how the statistical properties of the increments can be modified by adjusting the generator in a symmetrical fashion. Keeping fixed the endpoints (0, 0) and (1, 1), the middle turning points are changed into $(a, 2/3)$ and $(1 - a, 1/3)$ for $0 < a \leq 1/2$.

e. Percolation clusters (Stauffer and Aharony, 1992). Given a square lattice of side length L and a number $p \in [0, 1]$, assign a random number $x \in [0, 1]$ to each lattice cell and fill the cell if $x \leq p$. A *cluster* is a maximal collection of filled cells, connected by sharing common edges. Three examples are shown in Fig. 17. A

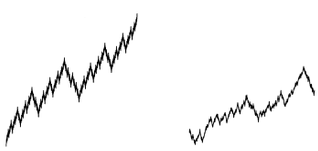

FIGURE 15 Left: The sixth iterate of the process of Fig. 14. Right: A sixth iterate of a randomized Brownian cartoon.

spanning cluster connects opposite sides of the lattice. For large L there is a *critical probability* or *percolation threshold* p_c; spanning clusters do not arise for $p < p_c$. Numerical experiments suggest $p_c \approx 0.59275$. In Fig. 17, $p = 0.4$, 0.6, and 0.8. Every lattice has its own p_c.

At $p = p_c$ the masses of the spanning clusters scale with the lattice size L as L^d, independently of the lattices. Experiment yields $d = 1.89 \pm 0.03$, and theory yields $d = 93/49$. This d is the mass dimension of Section II.C. In addition, spanning clusters have holes of all sizes; they are statistically self-similar fractals.

Many fractals are defined as part of a percolation cluster. The *backbone* is the subset of the spanning cluster that remains after removing all parts that can be separated from both spanned sides by removing a single filled cell from the spanning cluster. Numerical estimates suggest the backbone has dimension 1.61. The backbone is the path followed by a fluid diffusing through the lattice.

The *hull* of a spanning cluster is its boundary. It was observed by R. F. Voss in 1984 and proven by B. Duplantier that the hull's dimension is 7/4.

A more demanding definition of the boundary yields the *perimeter*. It was observed by T. Grossman and proven by B. Duplantier that the perimeter's dimension is 4/3.

Sapoval *et al.* (1985) examined discrete diffusion and showed that it involves a fractal diffusion front that can be modeled by the hull and the perimeter of a percolation cluster.

f. Diffusion-limited aggregation (DLA; Vicsek, 1992). DLA was proposed by Witten and Sander (1981, 1983) to simulate the aggregates that carbon particles form in a diesel engine. On a grid of square cells, a cartoon of DLA begins by occupying the center of the grid with a "seed particle." Next, place a particle in a square selected at random on the edge of a large circle centered on the seed square and let it perform a simple random walk. With each tick of the clock, with equal probabilities it will move to an adjacent square, left, right, above, or below. If the moving particle wanders too far from the seed, it falls off the edge of the grid and another wandering particle is started at a randomly chosen edge point. When a wandering particle reaches one of the four squares adjacent to the seed, it sticks to form a cluster of two particles, and another moving particle is released. When a moving particle reaches a square adjacent to the cluster, it sticks there. Continuing in this way builds an arbitrarily large object called a diffusion-limited aggregate (DLA) because the growth of the cluster is governed by the particles' diffusing across the grid. Figure 18 shows a moderate-size DLA cluster.

Early computer experiments on clusters of up to the 10^4 particles showed the mass $M(r)$ of the part of the cluster a distance r from the seed point scales as $M(r) \approx k \cdot r^d$,

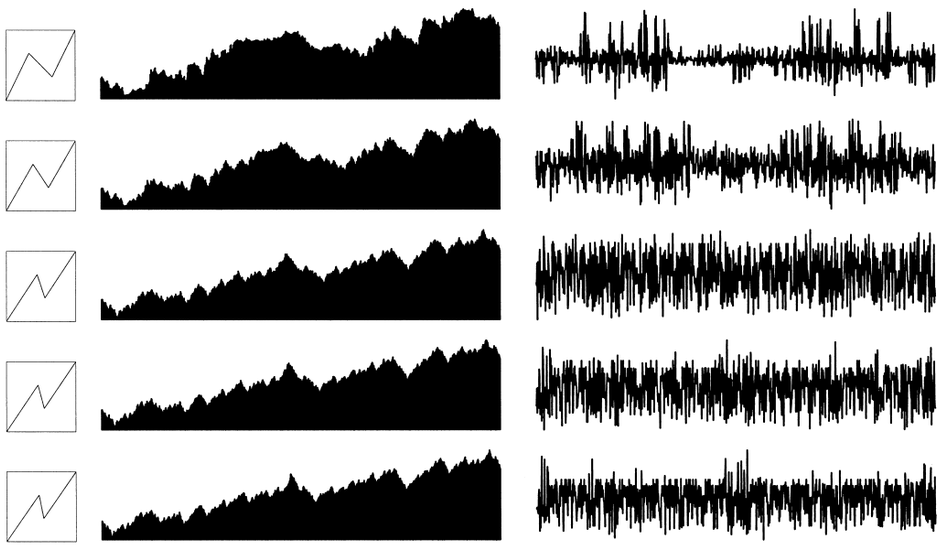

FIGURE 16 Generators, cartoons and difference graphs for symmetric cartoons with turning points $(a, 2/3)$ and $(1-a, 1/3)$, for $a = 0.333, 0.389, 0.444, 0.456,$ and 0.467. The same random number seed is used in all graphs.

with $d \approx 1.71$ for clusters in the plane and $d \approx 2.5$ for clusters in space. This exponent d is the mass dimension of the cluster. (See Sections II.C and V.) These values match measured scalings of physical objects moderately, but not terribly well. A careful examination of much larger clusters revealed discrepancies that added in due time to a very complex picture of DLA. Mandelbrot *et al.* (1995) investigated clusters in the 10^7 range; careful measurement reveals an additional dimension of 1.65 ± 0.01. This suggests the clusters become more compact as they grow. Also, as the cluster grows, more arms develop and the largest gaps decrease in size; i.e., the lacunarity decreases. (See Section VI.)

II. THE GENERIC NOTION OF FRACTAL DIMENSION AND A FEW SPECIFIC IMPLEMENTATIONS

The first, but certainly not the last, step in quantifying fractals is the computation of a dimension. The notion of Euclidean dimension has many aspects and therefore extends in several fashions. The extensions are distinct in the most general cases but coincide for exactly self-similar fractals. Many other dimensions cannot be mentioned here.

A more general approach to quantifying degrees of roughness is found in the article on *Multifractals*.

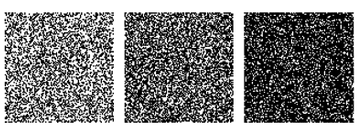

FIGURE 17 Percolation lattices well below, near, and well above the percolation threshold.

A. Similarity Dimension

The definition of similarity dimension is rooted in the fact that the unit cube in D-dimensional Euclidean space is self-similar: for any positive integer b the cube can be decomposed into $N = b^D$ cubes, each scaled by the similarity ratio $r = 1/b$, and overlapping at most along $(D-1)$-dimensional cubes.

The equiscaling or isoscaling case. Provided the pieces do not overlap significantly, the power-law relation $N = (1/r)^D$ between the number N and scaling factor r of the pieces generalizes to all exactly self-similar sets with all pieces scaled by the factor r. The *similarity dimension* d_{sim} is

$$d_{\text{sim}} = \frac{\log(N)}{\log(1/r)}.$$

FIGURE 18 A moderate-size DLA cluster.

The pluriscaling case. More generally, for self-similar sets where each piece is scaled by a possibly different factor r_i, the similarity dimension is the unique positive root d of the *Moran equation*

$$\sum_{i=1}^{N} r_i^d = 1.$$

The relation $0 \le d_{\text{sim}} \le E$. If the fractal is a subset of E-dimensional Euclidean space, E is called the *embedding dimension*.

So long as the overlap of the parts is not too great (technically, under the *open set condition*), we have $d_{\text{sim}} \le E$. If at least two of the r_i are positive, we have $d_{\text{sim}} > 0$. However, Section III.F shows that some circumstances introduce a latent dimension d, related indirectly to the similarity dimension, and that can satisfy $d < 0$ or $d > E$.

B. Box Dimension

The similarity dimension is meaningful only for exactly self-similar sets. For more general sets, including experimental data, it is often replaced by the box dimension. For any bounded (nonempty) set A in E-dimensional Euclidean space, and for any $\delta > 0$, a *δ-cover* of A is a collection of sets of diameter δ whose union contains A. Denote by $N_\delta(A)$ the smallest number of sets in a δ-cover of A. Then the *box dimension* d_{box} of A is

$$d_{\text{box}} = \lim_{\delta \to 0} \frac{\log(N_\delta(A))}{\log(1/\delta)}$$

when the limit exists. When the limit does not exist, the replacement of lim with lim sup and lim inf defines the *upper* and *lower box dimensions*:

$$\overline{d_{\text{box}}} = \limsup_{\delta \to 0} \frac{\log(N_\delta(A))}{\log(1/\delta)},$$

$$\underline{d_{\text{box}}} = \liminf_{\delta \to 0} \frac{\log(N_\delta(A))}{\log(1/\delta)}.$$

The box dimension can be thought of as measuring how well a set can be covered with small boxes of equal size, because the limit (or lim sup and lim inf) remain unchanged if $N_\delta(A)$ is replaced by the smallest number of E-dimensional cubes of side δ needed to cover A, or even the number of cubes of a δ lattice that intersect A.

Section V describes methods of measuring the box dimension for physical datasets.

C. Mass Dimension

The mass $M(r)$ of a d-dimensional Euclidean ball of constant density ρ and radius r is given by

$$M(r) = \rho \cdot V(d) \cdot r^d$$

$$\text{with} \quad V(d) = \left(\Gamma\left(\tfrac{1}{2}\right)^d\right) \Big/ \Gamma\left(d + \tfrac{1}{2}\right),$$

where $V(d)$ is the volume of the d-dimensional unit sphere. That is, for constant-density Euclidean objects, the ordinary dimension—among many other roles—is the exponent relating mass to size. This role motivated the definition of mass dimension for a fractal. The definition of mass is delicate. For example, the mass of a Sierpinski gasket cannot be defined by starting with a triangle of uniform density and removing middle triangles; this process would converge to a mass reduced to 0. One must, instead, proceed as on the left side of Fig. 1: take as initiator a triangle of mass 1, and as generator three triangles each scaled by $1/2$ and of mass $1/3$. Moreover, two very new facts come up.

Firstly, the $=$ sign in the formula for $M(r)$ must be replaced by $\approx$. That is, $M(r)$ fluctuates around a multiple of r^d. For example, as mentioned in Sections I.B.3.e and I.B.3.f, the masses of spanning percolation clusters and diffusion-limited aggregates scale as a power-law function of size. Consequently, the exponent in the relation $M(r) \approx k \cdot r^{d_{\text{mass}}}$ is called the *mass dimension*.

Second, in the Euclidean case the center is arbitrary but in the fractal case it must belong to the set under consideration. As an example, Fig. 19 illustrates attempts to measure the mass dimension of the Sierpinski gasket. Suppose we take circles centered at the lower left vertex of the initiator, and having radii $1/2$, $1/4, 1/8, \ldots$. We obtain $M(1/2^i) = 1/3^i = (1/2^i)^d$, where $d_{\text{mass}} = \log 3/\log 2$. See the left side of Fig. 19. That is, the mass dimension agrees with the similarity dimension.

On the other hand, if the circle's center is randomly selected in the interior of the initiator, the passage to the limit $r \to 0$ almost surely eventually stops with circles bounding no part of the gasket. See the middle of Fig. 19.

Taking a family of circles with center c a point of the gasket, the mass–radius relation becomes $M(r) = k(r, c) \cdot r^d$, where the prefactor $k(r, c)$ fluctuates and depends on both r and c. See the right side of Fig. 19. Even in this case, the exponent is the mass dimension. The prefactor is no longer a constant density, but a random variable, depending on the choice of the origin.

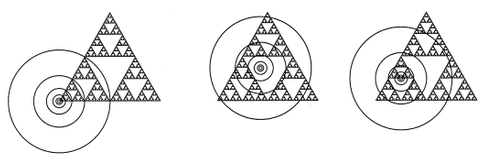

FIGURE 19 Attempts at measuring the mass dimension of a Sierpinski gasket using three families of circles.

Section V describes methods of measuring the mass dimension for physical datasets.

D. Minkowski–Bouligand Dimension

Given a set $A \subset \mathbf{R}^E$ and $\delta > 0$, the *Minkowski sausage* of A, also called the *δ-thickening* or *δ-neighborhood* of A, is defined as $A_\delta = \{x \in \mathbf{R}^E : d(x, y) \le \delta \text{ for some } y \in A\}$. (See Section I.B.b.) In the Euclidean case when A is a smooth m-dimensional manifold imbedded in $\mathbf{R}^E$, one has $vol(A_\delta) \sim \Lambda \cdot \delta^{E-m}$. That is, the E-dimensional volume of A_δ scales as δ to the codimension of A. This concept extends to fractal sets A: if the limit exists,

$$E - \lim_{\delta \to 0} \frac{\log(vol(A_\delta))}{\log(\delta)}$$

defines the *Minkowski–Bouligand dimension*, $d_{\mathrm{MB}}(A)$ (see Mandelbrot, 1982, p. 358). In fact, it is not difficult to see that $d_{\mathrm{MB}}(A) = d_{\mathrm{box}}(A)$. If the limit does not exist, lim sup gives $\overline{d_{\mathrm{box}}}(A)$ and lim inf gives $\underline{d_{\mathrm{box}}}(A)$.

In the privileged case when the limit

$$\lim_{\delta \to 0} \frac{vol(A_\delta)}{\delta^{E-m}}$$

exists, it generalizes the notion of Minkowski content for smooth manifolds A. Section VI will use this prefactor to measure lacunarity.

E. Hausdorff–Besicovitch Dimension

For a set A in Euclidean space, given $s \ge 0$ and $\delta > 0$, consider the quantity

$$\mathcal{H}^s_\delta(A) = \inf\left\{ \sum_i |U_i|^s : \{U_i\} \text{ is a } \delta\text{-cover of } A \right\}.$$

A decrease of δ reduces the collection of δ-covers of A, therefore $\mathcal{H}^s_\delta(A)$ increases as $\delta \to 0$ and $\mathcal{H}^s(A) = \lim_{\delta \to 0} \mathcal{H}^s_\delta(A)$ exists. This limit defines the *s-dimensional Hausdorff measure* of A. For $t > s$, $\mathcal{H}^t_\delta(A) \le \delta^{t-s} \mathcal{H}^s_\delta(A)$. It follows that a unique number d_{H} has the property that

$$s < d_{\mathrm{H}} \quad \text{implies} \quad \mathcal{H}^s(A) = \infty$$

and

$$s > d_{\mathrm{H}} \quad \text{implies} \quad \mathcal{H}^s(A) = 0.$$

That is,

$$d_{\mathrm{H}}(A) = \inf\{s : \mathcal{H}^s(A) = 0\} = \sup\{s : \mathcal{H}^s(A) = \infty\}.$$

This quantity d_{H} is the *Hausdorff–Besicovitch dimension* of A. It is of substantial theoretical significance, but in most cases is quite challenging to compute, even though it suffices to use coverings by disks. An upper bound often is relatively easy to obtain, but the lower bound can be much more difficult because the inf is taken over the collection of all δ-covers. Because of the inf that enters in its definition, the Hausdorff–Besicovitch dimension cannot be measured for any physical object.

Note: If A can be covered by $N_\delta(A)$ sets of diameter at most δ, then $\mathcal{H}^s_\delta(A) \le N_\delta(A) \cdot \delta^s$. From this it follows $d_{\mathrm{H}}(A) \le \underline{d_{\mathrm{box}}}(A)$, so $d_{\mathrm{H}}(A) \le d_{\mathrm{box}}(A)$ if $d_{\mathrm{box}}(A)$ exists. This inequality can be strict. For example, if A is any countable set, $d_{\mathrm{H}}(A) = 0$ and yet $d_{\mathrm{box}}(\text{rationals in } [0, 1]) = 1$.

F. Packing Dimension

Hausdorff dimension measures the efficiency of covering a set by disks of varying radius. Tricot (1982) introduced packing dimension to measure the efficiency of packing a set with disjoint disks of varying radius. Specifically, for $\delta > 0$ a *δ-packing* of A is a countable collection of disjoint disks $\{B_i\}$ with radii $r_i < \delta$ and with centers in A. In analogy with Hausdorff measure, define

$$\mathcal{P}^s_\delta(A) = \sup\left\{ \sum_i |B_i|^s : \{B_i\} \text{ is a } \delta\text{-packing of } A \right\}.$$

As δ decreases, so does the collection of δ-packings of A. Thus $\mathcal{P}^s_\delta(A)$ decreases as δ decreases and the limit

$$\mathcal{P}^s_0(A) = \lim_{\delta \to 0} \mathcal{P}^s_\delta(A)$$

exists. A technical complication requires an additional step. The *s-dimensional packing measure* of A is defined as

$$\mathcal{P}^s(A) = \inf\left\{ \sum_i \mathcal{P}^s_0(A_i) : A \subset \bigcup_{i=1}^{\infty} A_i \right\}.$$

Then the *packing dimension* $d_{\mathrm{pack}}(A)$ is

$$d_{\mathrm{pack}}(A) = \inf\{s : \mathcal{P}^s(A) = 0\} = \sup\{s : \mathcal{P}^s(A) = \infty\}.$$

Packing, Hausdorff, and box dimensions are related:

$$d_{\mathrm{H}}(A) \le d_{\mathrm{pack}}(A) \le \overline{d_{\mathrm{box}}}(A).$$

For appropriate A, each inequality is strict.

III. ALGEBRA OF DIMENSIONS AND LATENT DIMENSIONS

The dimensions of ordinary Euclidean sets obey several rules of thumb that are widely used, though rarely stated explicitly. For example, the union of two sets of dimension d and d' usually has dimension $\max\{d, d'\}$. The projection of a set of dimension d to a set of dimension d' usually gives a set of dimension $\min\{d, d'\}$. Also, for Cartesian products, the dimensions usually add:

$\dim(A \times B) = \dim(A) + \dim(B)$. For the intersection of subsets A and B of $\mathbf{R}^E$, it is the codimensions that usually add: $E - \dim(A \cap B) = (E - \dim(A)) + (E - \dim(B))$, but only so long as the sum of the codimensions is nonnegative. If this sum is negative, the intersection is empty. Mandelbrot (1984, Part II) generalized those rules to fractals and (see Section III.G) interpreted negative dimensions as measures of "degree of emptiness."

For simplicity, we restrict our attention to generaling these properties to the Hausdorff and box dimensions of fractals.

A. Dimension of Unions and Subsets

Simple applications of the definition of Hausdorff dimension give

$$A \subseteq B \quad \text{implies} \quad d_{\mathrm{H}}(A) \leq d_{\mathrm{H}}(B)$$

and

$$d_{\mathrm{H}}(A \cup B) = \max\{d_{\mathrm{H}}(A), d_{\mathrm{H}}(B)\}.$$

Replacing max with sup, this property holds for countable collections of sets. The subset and finite union properties hold for box dimension, but the countable union property fails.

B. Product and Sums of Dimensions

For all subsets A and B of Euclidean space, $d_{\mathrm{H}}(A \times B) \geq d_{\mathrm{H}}(A) + d_{\mathrm{H}}(B)$. Equality holds if one of the sets is sufficiently regular. For example, if $d_{\mathrm{H}}(A) = \overline{d_{\mathrm{H}}}(A)$, then $d_{\mathrm{H}}(A \times B) = d_{\mathrm{H}}(A) + d_{\mathrm{H}}(B)$. Equality does not always hold: Besicovitch and Moran (1945) give an example of subsets A and B of $\mathbf{R}$ with $d_{\mathrm{H}}(A) = d_{\mathrm{H}}(B) = 0$, yet $d_{\mathrm{H}}(A \times B) = 1$.

For upper box dimensions, the inequality is reversed: $\overline{d_{\mathrm{box}}}(A \times B) \leq \overline{d_{\mathrm{box}}}(A) + \overline{d_{\mathrm{box}}}(B)$.

C. Projection

Denote by $\mathrm{proj}_P(A)$ the projection of a set $A \subset \mathbf{R}^3$ to a plane $P \subset \mathbf{R}^3$ through the origin. If A is a one-dimensional Euclidean object, then for almost all choices of the plane P, $\mathrm{proj}_P(A)$ is one-dimensional. If A is a two- or three-dimensional Euclidean object, then for almost all choices of the plane P, $\mathrm{proj}_P(A)$ is two-dimensional of positive area. That is, $\dim(\mathrm{proj}_P(A)) = \min\{\dim(A), \dim(P)\}$.

The analogous properties hold for fractal sets A. If $d_{\mathrm{H}}(A) < 2$, then for almost all choices of the plane P, $d_{\mathrm{H}}(\mathrm{proj}_P(A)) = d_{\mathrm{H}}(A)$. If $d_{\mathrm{H}}(A) \geq 2$, then for almost all choices of the plane P, $d_{\mathrm{H}}(\mathrm{proj}_P(A)) = 2$ and $\mathrm{proj}_P(A)$ has positive area. So again, $d_{\mathrm{H}}(\mathrm{proj}_P(A)) = \min\{d_{\mathrm{H}}(A), d_{\mathrm{H}}(P)\}$.

The obvious generalization holds for fractals $A \subset \mathbf{R}^E$ and projections to k-dimensional hyperplanes through the origin.

Projections of fractals can be very complicated. There are fractal sets $A \subset \mathbf{R}^3$ with the surprising property that for almost every plane P through the origin, the projection $\mathrm{proj}_P(A)$ is any prescribed shape, to within a set of area 0. Consequently, as Falconer (1987) points out, in principle we could build a fractal digital sundial.

D. Subordination and Products of Dimension

We have already seen operations realizing the sum, max, and min of dimensions, and in the next subsection we shall examine the sum of codimensions. For certain types of fractals, multiplication of dimensions is achieved through "subordination," a process introduced in Bochner (1955) and elaborated in Mandelbrot (1982). Examples are constructed easily from the Koch curve generator (Fig. 20a). The initiator (the unit interval) is unchanged, but the new generator is a subset of the original generator. Figure 20 shows three examples.

In Fig. 20, generator (b) gives a fractal dust (B) of dimension $\log 3/\log 3 = 1$. Generator (c) gives the standard Cantor dust (C) of dimension $\log 2/\log 3$. Generator (d) gives a fractal dust (D) also of dimension $\log 2/\log 3$. Thinking of the Koch curve K as the graph of a function $f\colon [0, 1] \to K \subset \mathbf{R}^2$, the fractal (B) can be obtained by restricting f to the Cantor set with initiator $[0, 1]$ and generator the intervals $[0, 1/4]$, $[1/4, 1/2]$, and $[1/2, 3/4]$. In this case, the *subordinand* is a Koch curve, the *subordinator* is a Cantor set, and the *subordinate* is the fractal (B). The identity

$$\frac{\log 3}{\log 3} = \frac{\log 4}{\log 3} \cdot \frac{\log 3}{\log 4}$$

expresses that the dimensions multiply,

$$\dim(\text{subordinate}) = \dim(\text{subordinand}) \cdot \dim(\text{subordinator}).$$

Figure 20, (C) and (D) give other illustrations of this multiplicative relation. The *seeded universe* model of the distribution of galaxies (Section IX.D.1) uses subordination to obtain fractal dusts; see Mandelbrot (1982, plate 298).

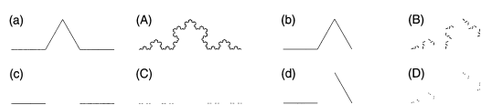

FIGURE 20 The Koch curve (A) and its generator (a); (b), (c), and (d) are subordinators, and the corresponding subordinates of the subordinand (A) are (B), (C), and (D).

E. Intersection and Sums of Codimension

The dimension of the intersection of two sets obviously depends on their relative placement. When $A \cap B = \emptyset$, the dimension vanishes. The following is a typical result. For Borel subsets A and B of $\mathbf{R}^E$, and for almost all $x \in \mathbf{R}^E$,

$$d_{\mathrm{H}}(A \cap (B + x)) \leq \max\{0, d_{\mathrm{H}}(A \times B) - E\}.$$

If $d_{\mathrm{H}}(A \times B) = d_{\mathrm{H}}(A) + d_{\mathrm{H}}(B)$, this reduces to

$$d_{\mathrm{H}}(A \cap (B + x)) \leq \max\{0, d_{\mathrm{H}}(A) + d_{\mathrm{H}}(B) - E\}.$$

This is reminiscent of the transversality relation for intersections of smooth manifolds.

Corresponding lower bounds are known in more restricted circumstances. For example, there is a positive measure set M of similarity transformations of $\mathbf{R}^E$ with

$$d_{\mathrm{H}}(A \cap T(B)) \geq d_{\mathrm{H}}(A) + d_H(B) - E$$

for all $T \in M$. Note $d_{\mathrm{H}}(A \cap T(B)) = d_{\mathrm{H}}(A) + d_{\mathrm{H}}(B) - E$ is equivalent to the addition of codimensions: $E - d_{\mathrm{H}}(A \cap T(B)) = (E - d_{\mathrm{H}}(A)) + (E - d_{\mathrm{H}}(B))$.

F. Latent Dimensions below 0 or above E

A blind application of the rule that codimensions are additive easily yields results that seem nonsensical, yet become useful if they are properly interpreted and the Hausdorff dimension is replaced by a suitable new alternative.

1. Negative Latent Dimensions as Measures of the "Degree of Emptiness"

Section E noted that if the codimension addition rule gives a negative dimension, the actual dimension is 0. This exception is an irritating complication and hides a feature worth underlining.

As background relative to the plane, consider the following intersections of two Euclidean objects: two points, a point and a line, and two lines. Naive intuition tells us that the intersection of two points is emptier than the intersection of a point and a line, and that the latter in turn is emptier than the intersection of two lines (which is almost surely a point). This informal intuition fails to be expressed by either a Euclidean or a Hausdorff dimension. On the other hand, the formal addition of codimensions suggests that the three intersections in question have the respective dimensions -2, -1, and 0. The inequalities between those values conform with the above-mentioned naive intuition. Therefore, they ushered in the search for a new mathematical definition of dimension that can be measured and for which negative values are legitimate and intuitive. This search produced several publications leading to Mandelbrot (1995). Two notions should be mentioned.

Embedding. A problem that concerns $\mathbf{R}^2$ can often be reinterpreted as a problem that really concerns $\mathbf{R}^E$, with $E > 2$, but must be approached within planar intuitions by $\mathbf{R}^2$. Conversely, if a given problem can be embedded into a problem concerning $\mathbf{R}^E$, the question arises, "which is the 'critical' value of $E - 2$, defined as the smallest value for which the intersection ceases to be empty, and precisely reduces to a point?" In the example of a line and a point, the critical $E - 2$ is precisely 1: once embedded in $\mathbf{R}^3$, the problem transforms into the intersection of a plane and a line, which is a point.

Approximation and pre-asymptotics in mathematics and the sciences. Consider a set defined as the limit of a sequence of decreasing approximations. When the limit is not empty, all the usual dimensions are defined as being properties of the limit, but when the limit is empty and all the dimensions vanish, it is possible to consider instead the limits of the properties of the approximations. The Minkowski–Bouligand formal definition of dimension generalizes to fit the naive intuitive values that may be either positive or negative.

2. Latent Dimensions That Exceed That of the Embedding Space

For a strictly self-similar set in $\mathbf{R}^E$, the Moran equation defines a similarity dimension that obeys $d_{\mathrm{sim}} \leq E$. On the other hand, a generator that is a self-avoiding broken line can easily yield $\log(N)/\log(1/r) = d_{\mathrm{sim}} > E$. Recursive application of this generator defines a parametrized motion, but the union of the positions of the motion is neither a self-similar curve nor any other self-similar set. It is, instead, a set whose points are covered infinitely often. Its box dimension is $\leq E$, which *a fortiori* is $< d_{\mathrm{sim}}$. However, one can load a mass on this set by following the route that applies in the absence of multiple points. Mass is distributed on the generator's intervals in proportion to the values of $r_i^{d_{\mathrm{sim}}}$. By infinite recursion, the difference between the times t' and t'' when points P' and P'' are visited is defined as the mass supported by the portion of the curve that links these points.

If so and $d_{\mathrm{sim}} > E$, the similarity dimension acquires a useful role as a latent dimension. For example, consider the multiplication of dimensions in Section III.D. Suppose that our recursively constructed set is not lighted for all instants of time, but only intermittently when time falls within a fractal dust of dimension d''. Then, the rule of thumb is that the latent dimension of the lighted points is $d_{\mathrm{sim}}d''$. When $d_{\mathrm{sim}}d'' < E$, the rule of thumb is that the true dimension is also $d_{\mathrm{sim}}d''$.

Figure 21 shows an example. The generator has $N = 6$ segments, each with scaling ratio $r = 1/2$, hence latent dimension $d_{\mathrm{sim}} = \log 6/\log 2 > 2$. Taking as subordinator

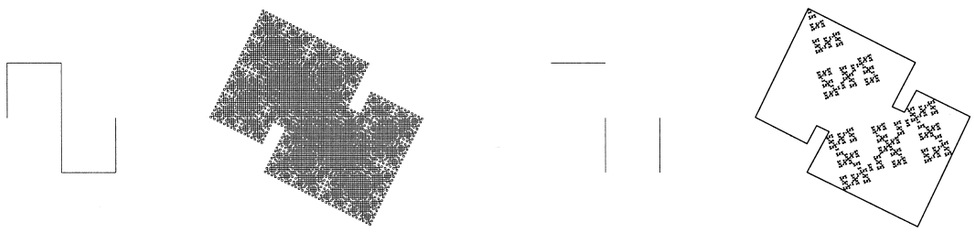

FIGURE 21 Left: Generator and limiting shape with latent dimension exceeding 2. Right: generator and limiting shape of a subordinate with dimension <2. For comparison, this limiting shape is enclosed in the outline of the left limiting shape.

a Cantor set with generator having $N = 3$ segments, each with scaling ratio $r = 1/2$, yields a self-similar fractal with dimension $\log 3/\log 2$.

G. Mapping

Recall f satisfies the Hölder condition with exponent H if there is a positive constant c for which $|f(x) - f(y)| \le c|x - y|^H$. For such functions, $d_{\mathrm{H}}(f(A)) \le (1/H)d_{\mathrm{H}}(A)$. If $H = 1$, f is called a Lipschitz function; f is bi-Lipschitz if there are constants c_1 and c_2 with $c_1|x - y| \le |f(x) - f(y)| \le c_2|x - y|$. Hausdorff dimension is invariant under bi-Lipschitz maps. The analogous properties hold for box-counting dimension.

IV. METHODS OF COMPUTING DIMENSION IN MATHEMATICAL FRACTALS

Upper bounds for the Hausdorff dimension can be relatively straightforward: it suffices to consider a specific family of coverings of the set. Lower bounds are more delicate. We list and describe briefly some methods for computing dimension.

A. Mass Distribution Methods

A *mass distribution* on a set A is a measure μ with $\mathrm{supp}(\mu) \subset A$ and $0 < \mu(A) < \infty$. The *mass distribution principle* (Falconer, 1990, p. 55) establishes a lower bound for the Hausdorff dimension: Let μ be a mass distribution on A and suppose for some s there are constants $c > 0$ and $\delta > 0$ with $\mu(U) \le c \cdot |U|^s$ for all sets U with $|U| \le \delta$. Then $\delta \le d_{\mathrm{H}}(A)$.

Suitable choice of mass distribution can show that no individual set of a cover can cover too much of A. This can eliminate the problems caused by covers by sets of a wide range of diameters.

B. Potential Theory Methods

Given a mass distribution μ, the *s-potential* is defined by Frostman (1935) as

$$\phi_s(x) = \int \frac{d\mu(x)}{|x - y|^s}.$$

If there is a mass distribution μ on a set A with $\int \phi_s(x)\, d\mu(x) < \infty$, then $d_{\mathrm{H}}(A) \ge s$. Potential theory has been useful for computing dimension of many sets, for example, Brownian paths.

C. Implicit Methods

McLaughlin (1987) introduced a geometrical method, based on local approximate self-similarities, which succeeds in proving that $d_{\mathrm{H}}(A) = \overline{d_{\mathrm{box}}}(A)$, without first determining $d_{\mathrm{H}}(A)$. If small parts of A can be mapped to large parts of A without too much distortion, or if A can be mapped to small parts of A without too much distortion, then $d_{\mathrm{H}}(A) = \overline{d_{\mathrm{box}}}(A) = s$ and $\mathcal{H}^s(A) > 0$ (in the former case) or $\mathcal{H}^s(A) < \infty$ (in the latter case). Details and examples can be found in Falconer (1997, Section 3.1).

D. Thermodynamic Formalism

Sinai (1972), Bowen (1975), and Ruelle (1978) adapted methods of statistical mechanics to determine the dimensions of fractals arising from some nonlinear processes. Roughly, for a fractal defined as the attractor A of a family of nonlinear contractions F_i with an inverse function f defined on A, the *topological pressure* $P(\phi)$ of a Lipschitz function ϕ: $A \to \mathbf{R}$ is

$$P(\phi) = \lim_{k\to\infty} \frac{1}{k} \log \left\{ \sum_{x \in \mathrm{Fix}(f^k)} \exp[\phi(x) + \phi(f(x)) + \cdots \phi(f^{k-1}(x))] \right\},$$

where $\mathrm{Fix}(f^k)$ denotes the set of fixed points of f^k. The sum plays the role of the partition function in statistical mechanics, part of the motivation for the name "thermodynamic formalism." There is a unique s for which

$P(-s\log|f'|)=0$, and $s=d_{\mathrm{H}}(A)$. Under these conditions, $0<\mathcal{H}^s(A)<\infty$, $\mathcal{H}^s(A)$ is a Gibbs measure on A, and many other results can be deduced. Among other places, this method has been applied effectively to the study of Julia sets.

V. METHODS OF MEASURING DIMENSION IN PHYSICAL SYSTEMS

For shapes represented in the plane—for example, coastlines, rivers, mountain profiles, earthquake faultlines, fracture and cracking patterns, viscous fingering, dielectric breakdown, growth of bacteria in stressed environments—box dimension is often relatively easy to compute. Select a sequence $\epsilon_1>\epsilon_2>\cdots>\epsilon_n$ of sizes of boxes to be used to cover the shape, and denote by $N(\epsilon_i)$ the number of boxes of size ϵ_i needed to cover the shape. A plot of $\log(N(\epsilon_i))$ against $\log(1/\epsilon_i)$ often reveals a scaling range over which the points fall close to a straight line. In the presence of other evidence (hierarchical visual complexity, for example), this indicates a fractal structure with box dimension given by the slope of the line. Interpreting the box dimension in terms of underlying physical, chemical, and biological processes has yielded productive insights.

For physical objects in three-dimensional space—for example, aggregates, dustballs, physiological branchings (respiratory, circulatory, and neural), soot particles, protein clusters, terrain maps—it is often easier to compute mass dimension. Select a sequence of radii $r_1>r_2>\cdots>r_n$ and cover the object with concentric spheres of those radii. Denoting by $M(r_i)$ the mass of the part of the object contained inside the sphere of radius r_i, a plot of $\log(M(r_i))$ against $\log(r_i)$ often reveals a scaling range over which the points fall close to a straight line. In the presence of other evidence (hierarchical arrangements of hole sizes, for example), this indicates a fractal structure with mass dimension given by the slope of the line. Mass dimension is relevant for calculating how density scales with size, and this in turn has implications for how the object is coupled to its environment.

VI. LACUNARITY

Examples abound of fractals sharing the same dimension but looking quite different. For instance, both Sierpinski carpets in Fig. 22 have dimension $\log 40/\log 7$. The holes' distribution is more uniform on the left than on the right. The quantification of this difference was undertaken in Mandelbrot (1982, Chapter 34). It introduced *lacunarity* as one expression of this difference, and took another step in characterizing fractals through associated numbers. How can the distribution of a fractal's holes or gaps ("lacunae") be quantified?

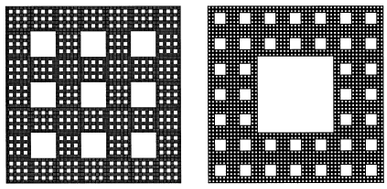

FIGURE 22 Two Sierpinski carpet fractals with the same dimension.

A. The Prefactor

Suppose A is either carpet in Fig. 22, and let A_δ denote the δ-thickening of A. As mentioned in Section II.D, $\mathrm{area}(A_\delta)\sim\Lambda\cdot\delta^{2-\log 40/\log 7}$. One measure of lacunarity is $1/\Lambda$, if the appropriate limit exists.

It is well known that for the box dimension, the limit as $\epsilon\to 0$ can be replaced by the sequential limit $\epsilon_n\to 0$, for ϵ_n satisfying mild conditions. For these carpets, natural choices are those ϵ_n just filling successive generations of holes. Applied to Fig. 22, these ϵ_n give $1/\Lambda\approx 0.707589$ and 0.793487, agreeing with the notion that higher lacunarity corresponds to a more uneven distribution of holes.

Unfortunately, the prefactor is much more sensitive than the exponent: different sequences of ϵ_n give different limits. Logarithmic averages can be used, but this is work in progress.

B. The Crosscuts Structure

An object is often best studied through its *crosscuts* by straight lines, concentric circles, or spheres. For a fractal of dimension d in the plane, the rule of thumb is that the crosscuts are Cantor-like objects of dimension $d-1$. The case when the gaps between points in the crosscut are statistically independent was singled out by Mandelbrot as defining "neutral lacunarity." If the crosscut is also self-similar, it is a Lévy dust.

Hovi *et al.* (1996) studied the intersection of lines (linear crosscuts) with two- and three-dimensional critical percolation clusters, and found the gaps are close to being statistically independent, thus a Lévy dust.

In studying very large DLA clusters, Mandelbrot *et al.* (1995) obtained a crosscut dimension of $d_c=0.65\pm 0.01$, different from the value 0.71 anticipated if DLA clusters were statistically self-similar objects with mass dimension $d_{\mathrm{mass}}=1.71$. The difference can be explained by asserting the number of particles $N_c(r/l)$ on a crosscut

of radius r scales as $N_c(r/l) = \Lambda(r)(r/l)^{d_c}$. Here l is the scaling length, and the lacunarity prefactor varies with r. Assuming slow variation of $\Lambda(r)$ with r, the observed linear log–log fit requires $\Lambda(r) \sim r^{\delta d}$, where $\delta d = d_{\text{mass}} - 1 - d_c = 0.06 \pm 0.01$. Transverse crosscut analysis reveals lacunarity decreases with r for large DLA clusters.

C. Antipodal Correlations

Select an occupied point p well inside a random fractal cluster, so that the $R \times R$ square centered at p lies within the cluster. Now select two vectors V and W based at p and separated by the angle θ. Finally, denote by x and y the number of occupied sites within the wedges with apexes at p, apex angles ϕ much less than θ, and centered about the vectors V and W. The *angular correlation function* is

$$C(\theta) = \frac{\langle xy \rangle - \langle x \rangle \langle y \rangle}{\langle x^2 \rangle - \langle x \rangle \langle x \rangle},$$

where $\langle \cdots \rangle$ denotes an average over many realizations of the random fractal. *Antipodal correlations* concern $\theta = \pi$. Negative and positive antipodal correlations are interpreted as indicating high and low lacunarity; vanishing correlation is a weakened form of neutral lacunarity.

Mandelbrot and Stauffer (1994) used antipodal correlations to study the lacunarity of critical percolation clusters. On smaller central subclusters, they found the antipodes are uncorrelated.

Trema random fractals. These are formed by removing randomly centered discs, tremas, with radii obeying a power-law scaling. For them, $C(\pi) \to 0$ with ϕ because a circular hole that overlaps a sector cannot overlap the opposite sector. But nonconvex tremas introduce positive antipodal correlations. For θ close to π, needle-shaped tremas, though still convex, yield $C(\theta)$ much higher than for circular trema sets. From this more refined viewpoint, needle tremas' lacunarity is much lower.

VII. FRACTAL GRAPHS AND SELF-AFFINITY

A. Weierstrass Functions

Smooth functions' graphs, as seen under sufficient magnification, are approximated by their tangents. Unless the function itself is linear, the existence of a tangent contradicts the scale invariance that characterizes fractals. The early example of a continuous, nowhere-differentiable function devised in 1834 by Bolzano remained unpublished until the 1920s. The first example to become widely known was constructed by Weierstrass in 1872. The *Weierstrass sine function* is

$$W(t) = \sum_{n=0}^{\infty} b^{-Hn} \sin(2\pi b^n t),$$

and the complex *Weierstrass function* is

$$W_0(t) = \sum_{n=0}^{\infty} b^{-Hn} \exp(2\pi i b^n t).$$

Hardy (1916) showed $W(t)$ is continuous and nowhere-differentiable if and only if $b > 1$ and $0 < H < 1$.

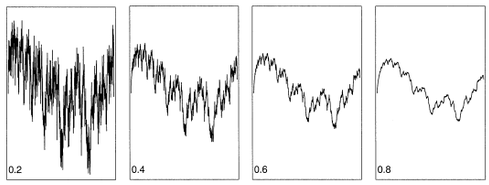

FIGURE 23 The effect of H on Weierstrass graph roughness. In all pictures, $b = 1.5$ and H has the indicated value.

As shown in Fig. 23, the parameter H determines the roughness of the graph. In this case, H is not a perspicuous "roughness exponent." Indeed, as b increases, the amplitudes of the higher frequency terms decrease and the graph is more clearly dominated by the lowest frequency terms. This effect of b is a little-explored aspect of lacunarity.

B. Weierstrass–Mandelbrot Functions

The Weierstrass function revolutionized mathematics but did not enter physics until it was modified in a series of steps described in Mandelbrot (1982, pp. 388–390; (2001d, Chapter H4). The step from $W_0(t)$ to $W_1(t)$ added low frequencies in order to insure self-affinity. The step from $W_1(t)$ to $W_2(t)$ added to each addend a random phase φ_n uniformly distributed on [0, 1]. The step from $W_1(t)$ to $W_3(t)$ added a random amplitude $A_n = \sqrt{-2 \log V}$, where V is uniform on [0, 1]. A function $W_4(t)$ that need not be written down combines a phase and an amplitude. The latest step leads to another function that need not be written down: it is $W_5(t) = W_4(t) + W_4(-t)$, where the two addends are statistically independent. Contrary to all earlier extensions, $W_5(t)$ is not chiral. We have

$$W_1(t) = \sum_{n=-\infty}^{\infty} b^{-Hn}(\exp(2\pi i b^n t) - 1),$$

$$W_2(t) = \sum_{n=-\infty}^{\infty} b^{-Hn}(\exp(2\pi i b^n t) - 1)\exp(i\varphi_n),$$

$$W_3(t) = \sum_{n=-\infty}^{\infty} A_n b^{-Hn}(\exp(2\pi i b^n t) - 1).$$

C. The Hölder Exponent

A function $f: [a, b] \to \mathbf{R}$ has *Hölder exponent* H if there is a constant $c > 0$ for which

$$|f(x) - f(y)| \leq c \cdot |x - y|^H$$

for all x and y in $[a, b]$ (recall Section III.G). If f is continuous and has Hölder exponent H satisfying $0 < H \leq 1$, then the graph of f has box dimension $d_{\text{box}} \leq 2 - H$.

The Weierstrass function $W(t)$ has Hölder exponent H, hence its graph has $d_{\text{box}} \leq 2 - H$. For large enough b, $d_{\text{box}} = 2 - H$, so one can think of the Hölder exponent as a measure of roughness of the graph.

VIII. FRACTAL ATTRACTORS AND REPELLERS OF DYNAMICAL SYSTEMS

The modern renaissance in dynamical systems is associated most often with chaos theory. Consequently, the relations between fractal geometry and chaotic dynamics, mediated by symbolic dynamics, are relevant to our discussion. In addition, we consider fractal basin boundaries, which generalize Julia sets to much wider contexts including mechanical systems.

A. The Smale Horseshoe

If they exist, intersections of the stable and unstable manifolds of a fixed point are called *homoclinic points*. Poincaré (1890) recognized that homoclinic points cause great complications in dynamics. Yet much can be understood by labeling an appropriate coarse-graining of a neighborhood of a homoclinic point and translating the corresponding dynamics into a string of symbols (the coarse-grain bin labels). The notion of symbolic dynamics first appears in Hadamard (1898), and Birkhoff (1927) proved every neighborhood of a homoclinic point contains infinitely many periodic points.

Motivated by work of Cartwright and Littlewood (1945) and Levinson (1949) on the forced van der Pol oscillator, Smale (1963) constructed the *horseshoe map*. This is a map from the unit square into the plane with completely invariant set a Cantor set Λ, roughly the Cartesian product of two Cantor middle-thirds sets. Restricted to Λ, with the obvious symbolic dynamics encoding, the horseshoe map is conjugate to the shift map on two symbols, the archetype of a chaotic map.

This construction is universal in the sense that it occurs in every transverse homoclinic point to a hyperbolic saddle point. The Conley–Moser theorem (see Wiggins, 1990) establishes the existence of chaos by conjugating the dynamics to a shift map on a Cantor set under general conditions. In this sense, chaos often equivalent to simple dynamics on an underlying fractal.

B. Fractal Basin Boundaries

For any point c belonging to a hyperbolic component of the Mandelbrot set, the Julia set is the boundary of the basins of attraction of the attracting cycle and the attracting fixed point at infinity. See the right side of Fig. 3.

Another example favored by Julia is found in Newton's method for finding the roots of a polynomial $f(z)$ of degree at least 3. It leads to the dynamical system $z_{n+1} = N_f(z_n) = z_n - f(z_n)/f'(z_n)$. The roots of $f(z)$ are attracting fixed points of $N_f(z)$, and the boundary of the basins of attraction of these fixed points is a fractal; an example is shown on the left side of Fig. 24. If contaminated by even small uncertainties, the fate of initial points near the basin boundary cannot be predicted. Sensitive dependence on initial conditions is a signature of chaos, but here we deal with something different. The eventual behavior is completely predictable, except for initial points taken exactly on the basin boundary, usually of two-dimensional Lebesgue measure 0.

The same complication enters mechanical engineering problems for systems with multiple attractors. Moon (1984) exhibited an early example. Extensive theoretical and computer studies by Yorke and coworkers are described in Alligood and Yorke (1992). The driven harmonic oscillator with two-well potential

$$\frac{d^2x}{dt^2} + f\frac{dx}{dt} - \frac{1}{2}x(1 - x^2) = A\cos(\omega t)$$

is a simple example. The undriven system has two equilibria, $x = -1$ and $x = +1$. Initial values (x, x') are painted white if the trajectory from that point eventually stays in the left basin, black if it eventually stays in the right basin. The right side of Fig. 24 shows the initial condition portrait for the system with $f = 0.15$, $\omega = 0.8$, and $A = 0.094$.

IX. FRACTALS AND DIFFERENTIAL OR PARTIAL DIFFERENTIAL EQUATIONS

The daunting task to which a large portion of Mandelbrot (1982) is devoted was to establish that many works of nature and man [as shown in Mandelbrot (1997), the latter includes the stock market!] are fractal. New and often important examples keep being discovered, but the hardest present challenge is to discover the *causes* of fractality. Some cases remain obscure, but others are reasonably clear.

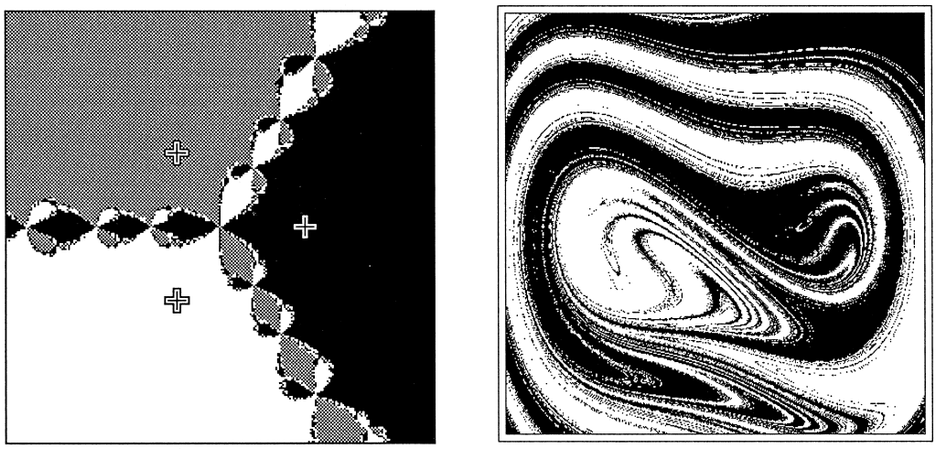

FIGURE 24 Left: The basins of attraction of Newton's method for finding the roots of $z^3 - 1$. Right: The basins of attraction for a damped, driven two-well harmonic oscillator.

Thus, the fractality of the physical percolation clusters (Section I.B.3.e) is the geometric counterpart of scaling and renormalization: the analytic properties of those objects follow a wealth of power-law relations. Many mathematical issues, some of them already mentioned, remain open, but the overall renormalization framework is firmly rooted. Renormalization and the resulting fractality also occur in the structure of attractors and repellers of dynamical systems. Best understood is renormalization for quadratic maps. Feigenbaum and others considered the real case. For the complex case, renormalization establishes that the Mandelbrot set contains infinitely many small copies of itself.

Unfortunately, additional examples of fractality proved to be beyond the scope of the usual renormalization. A notorious case concerns DLA (Section I.B.3.f).

A. Fractal Attractors of Ordinary Differential Equations

The Lorenz equations for fluid convection in a two-dimensional layer heated from below are

$$\frac{dx}{dt} = \sigma(y-x), \quad \frac{dy}{dt} = -xz+rx-y, \quad \frac{dz}{dt} = xy-bz.$$

Here x denotes the rate of convective overturning, y the horizontal temperature difference, and z the departure from a linear vertical temperature gradient. For the parameters $\sigma = 10$, $b = 8/3$, and $r = 28$, Lorenz (1963) suggested that trajectories in a bounded region converge to an attractor that is a fractal, with dimension about 2.06, as estimated by Liapunov exponents. The Lorenz equations are very suggestive but do not represent weather systems very well. However, Haken established a connection with lasers. The sensitivity to initial conditions common to chaotic dynamics is mediated by the intricate fractal interleaving of the multiple layers of the attractor. In addition, Birman and Williams (1983) showed an abundance of knotted periodic orbits embedded in the Lorenz attractor, though Williams (1983) showed all such knots are prime. Grist (1997) constructed a *universal template*, a branched 2-manifold in which all knots are embedded. Note the interesting parallel with the universal aspects of the Sierpinski carpet (Section I.B.1.a). It is not yet known if the attractor of any differential equation contains a universal template. The Poincaré–Bendixson theorem prohibits fractal attractors for differential equations in the plane, but many other classical ordinary differential equations in at least three dimensions exhibit similar fractal attractors in certain parameter ranges.

B. Partial Differential Equations on Domains with Fractal Boundaries ("Can One Hear the Shape of a Fractal Drum?")

Suppose $D \subset \mathbf{R}^n$ is an open region with boundary ∂D. Further, suppose the eigenvalue problem $\nabla^2 u = -\lambda u$ with boundary conditions $u(x) = 0$ for all $x \in \partial D$ has real eigenvalues $0 < \lambda_1 < \lambda_2 < \cdots$. For D with sufficiently smooth boundary, a theorem of Weyl (1912) shows $N(\lambda) \sim \lambda^{n/2}$, where the *eigenvalue counting function* $N(\lambda) = \{\text{the number of } \lambda_i \text{ for which } \lambda_i \leq \lambda\}$. If the boundary ∂D is a fractal, Berry (1979, pp. 51–53) postulated that some form of the dimension of ∂D appears in the second term in the expansion of $N(\lambda)$, therefore can be recovered from the eigenvalues. This *could not* be the Hausdorff dimension, but Lapidus (1995) showed that it

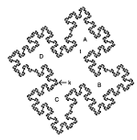

FIGURE 25 Perimeter of an extensively studied fractal drum.

is the Minkowski–Bouligard dimension. The analysis is subtle, involving some deep number theory.

For regions with fractal boundaries, the heat equation $\nabla^2 u = (\partial/\partial t)u$ shows heat flow across a fractal boundary is related to the dimension of the boundary. Sapoval (1989) and Sapoval *et al*. (1991) conducted elegant experiments to study the modes of fractal drums. The perimeter of Fig. 25 has dimension $\log 8/\log 4 = 3/2$. A membrane stretched across this fractal curve was excited acoustically and the resulting modes observed by sprinkling powder on the membrane and shining laser light transverse to the surface. Sapoval observed modes localized to bounded regions A, B, C, and D shown in Fig. 25. By carefully displacing the acoustic source, he was able to excite each separately.

Theoretical and computer-graphic analyses of the wave equation on domains with fractal boundaries have been carried out by Lapidus *et al*. (1996), among others.

C. Partial Differential Equations on Fractals

The problem is complicated by the fact that a fractal is not a smooth manifold. How is the Laplacian to be defined on such a space? One promising approach was put forward by physicists in the 1980s and made rigorous in Kigami (1989): approximate the fractal domain by a sequence of graphs representing successive protofractals, and define the fractal Laplacian as the limit of a suitably renormalized sequence of Laplacians on the graphs. Figure 26 shows the first four graphs for the equilateral Sierpinski gasket. The values at the boundary vertices are specified by the boundary conditions at any nonboundary vertex x_0. The mth approximate Laplacian of a function $f(x)$ is the product of a renormalization factor by $\sum (f(y) - f(x_0))$, where the sum is taken over all vertices y in the mth protofractal graph corresponding to the mth-stage reduction of the whole graph.

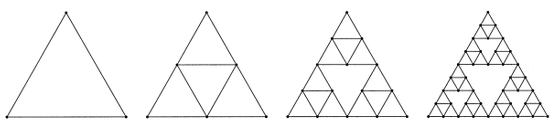

FIGURE 26 Graphs corresponding to protofractal approximations of the equilateral Sierpinski gasket.

With this Laplacian, the heat and wave equations can be defined on fractals. Among other things, the wave equation on domains with fractal boundaries admits localized solutions, as we saw for the wave equation on fractal drums. A major challenge is to extend these ideas to fractals more complicated than the Sierpinski gasket and its relatvives.

D. How Partial Differential Equations Generate Fractals

A quandary: It is universally granted that physics is ruled by diverse partial differential equations, such as those of Laplace, Poisson, and Navier–Stokes. A differential equation necessarily implies a great degree of local smoothness, even though close examination shows isolated singularities or "catastrophes." To the contrary, fractality implies everywhere-dense roughness or fragmentation. This is one of the several reasons that fractal models in diverse fields were initially perceived as being "anomalies" contradicting one of the firmest foundations of science.

A conjecture–challenge responding to the preceding quandry. There is no contradiction at all: fractals arise unavoidably in the long-time behavior of the solution of very familiar and innocuous-looking equations. In particular, many concrete situations where fractals are observed involve equations that allow free and moving boundaries, interfaces, or singularities. As a suggestive "principle," Mandelbrot (1982, Chapter 11) described the following possibility: under broad conditions that largely remain to be specified, these free boundaries, interfaces, and singularities converge to suitable fractals. Many equations have been examined from this viewpoint, but we limit ourselves to two examples of central importance.

1. The Large-Scale Distribution of Galaxies

Chapters 9 and 33–35 of Mandelbrot (1982) conjecture that the distribution of galaxies is fractal. This conjecture results from a search for invariants that was central to every aspect of the construction of fractal geometry. Granted that the distribution of galaxies certainly deviates from homogeneity, one broad approach consists in correcting for local inhomogeneity by using local "patches." The next simplest global assumption is that the distribution is nonhomogeneous but scale invariant, therefore fractal.

Excluding the strict hierarchies, two concrete constructions of random fractal sets were subjected to detailed mathematical and visual investigation. These constructions being random, self-similarity can only be statistical. But a strong counteracting asset is that the self-similarity ratio can be chosen freely, is not restricted to powers of a prescribed r_0. A surprising and noteworthy finding came forth. These constructions exhibited a strong hierarchical

structure that is not a deliberate and largely arbitrary input. Details are given in Mandelbrot (1982).

The first construction is the *seeded universe* based on a Lévy flight. Its Hausdorff-dimensional properties were well known. Its correlation properties (Mandelbrot 1975) proved to be nearly identical to those of actual galaxy maps. The second construction is the *parted universe* obtained by subtracting from space a random collection of overlapping tremas. Either construction yields sets that are highly irregular and involve no special center, yet, with no deliberate design, exhibit a clear-cut clustering, "filaments" and "walls." These structures were little known when these constructions were designed.

Conjecture: Could it be that the observed "clusters," "filaments," and "walls" need not be explained separately? They may not result from unidentified features of specific models, but represent unavoidable consequences of a variety of unconstrained forms of random fractality, as interpreted by a human brain.

A problem arose when careful examination of the simulations revealed a clearly incorrect prediction. The simulations in the *seeded universe* proved to be visually far more "lacunar" than the real world. That is, the simulations' holes are larger than in reality. The *parted universe* model fared better, since its lacunarity can be adjusted at will and fit to the actual distribution. A lowered lacunarity is expressed by a positive correlation between masses in antipodal directions. Testing this specific conjecture is a challenge for those who analyze the data.

Does dynamics make us expect the distribution of galaxies to be fractal? Position a large array of point masses in a cubic box in which opposite sides are identified to form a three-dimensional torus. The evolution of this array obeys the Laplace equation, with the novelty that the singularities of the solution are the positions of the points, therefore movable. All simulations we know (starting with those performed at IBM around 1960) suggest that, even when the pattern of the singularities begins by being uniform or Poisson, it gradually creates clusters and a semblance of hierarchy, and appears to tend toward fractality. It is against the preceding background that the limit distribution of galaxies is conjectured to be fractal, and fractality is viewed as compatible with Newton's equations.

2. The Navier–Stokes Equation

The first concrete use of a Cantor dust in real spaces is found in Berger and Mandelbrot (1963), a paper on noise records. This was nearly simultaneous with Kolmogorov's work on the intermittence of turbulence. After numerous experimental tests designed to create an intuitive feeling for this phenomenon (e.g., listening to turbulent velocity records that were made audible), the fractal viewpoint was extended to turbulence, and circa 1964 led to the following conjecture.

Conjecture. The property of being "turbulently dissipative" should not be viewed as attached to domains in a fluid with significant interior points, but as attached to fractal sets. In a first approximation, those sets' intersection with a straight line is a Cantor-like fractal dust having a dimension in the range from 0.5 to 0.6. The corresponding full sets in space should therefore be expected to be fractals with Hausdorff dimension in the range from 2.5 to 2.6.

Actually, Cantor dust and Hausdorff dimension are not the proper notions in the context of viscous fluids because viscosity necessarily erases the fine detail essential to fractals. Hence the following conjecture (Mandelbrot, 1982, Chapter 11; 1976). The dissipation in a viscous fluid occurs in the neighborhood of a singularity of a nonviscous approximation following Euler's equations, and the motion of a nonviscous fluid acquires singularities that are sets of dimension about 2.5–2.6. Several numerical tests agree with this conjecture (e.g., Chorin, 1981).

A related conjecture, that the Navier–Stokes equations have fractal singularities of much smaller dimension, has led to extensive work by V. Scheffer, R. Teman, and C. Foias, and many others. But this topic is not exhausted.

Finally, we mention that fractals in phase space entered the transition from laminar to turbulent flow through the work of Ruelle and Takens (1971) and their followers. The task of unifying the real- and phase-space roles of fractals is challenging and far from being completed.

X. FRACTALS IN THE ARTS AND IN TEACHING

The Greeks asserted art reflects nature, so it is little surprise that the many fractal aspects of nature should find their way into the arts—beyond the fact that a representational painting of a tree exhibits the same fractal branching as a physical tree. Voss and Clarke (1975) found fractal power-law scaling in music, and self-similarity is designed in the music of the composers György Ligeti and Charles Wuorinen. Pollard-Gott (1986) established the presence of fractal repetition patterns in the poetry of Wallace Stevens. Computer artists use fractals to create both abstract aesthetic images and realistic landscapes. Larry Poons' paintings since the 1980s have had rich fractal textures. The "decalcomania" of the 1830s and the 1930s and 1940s used viscous fingering to provide a level of visual complexity. Before that, Giacometti's Alpine wildflower paintings are unquestionably fractal. Earlier still, relatives of the Sierpinski gasket occur as decorative motifs in Islamic and Renaissance art. Fractals abound in architecture, for example, in the cascades of spires in Indian temples, Bramante's

plan for St. Peter's, Malevich's Architektonics, and some of Frank Lloyd Wright's designs. Fractals occur in the writing of Clarke, Crichton, Hoag, Powers, Updike, and Wilhelm, among others, and in at least one play, Stoppard's *Arcadia*. Postmodern literary theory has used some concepts informed by fractal geometry, though this application has been criticized for its overly free interpretations of precise scientific language. Some have seen evidence of power-law scaling in historical records, the distribution of the magnitudes of wars and of natural disasters, for example. In popular culture, fractals have appeared on t-shirts, totebags, book covers, MTV logos, been mentioned on public radio's *A Prairie Home Companion*, and been seen on television programs from *Nova* and *Murphy Brown*, through several incarnations of *Star Trek*, to *The X-Files* and *The Simpsons*. While Barnsley's (1988) slogan, "fractals everywhere," is too strong, the degree to which fractals surround us outside of science and engineering is striking.

A corollary of this last point is a good conclusion to this high-speed survey. In our increasingly technological world, science education is very important. Yet all too often humanities students are presented with limited choices: the first course in a standard introductory sequence, or a survey course diluted to the level of journalism. The former builds toward major points not revealed until later courses, the latter discusses results from science without showing how science is done. In addition, many efforts to incorporate computer-aided instruction attempt to replace parts of standard lectures rather than engage students in exploration and discovery.

Basic fractal geometry courses for non-science students provide a radical departure from this mode. The subject of fractal geometry operates at human scale. Though new to most, the notion of self-similarity is easy to grasp, and (once understood) handles familiar objects from a genuinely novel perspective. Students can explore fractals with the aid of readily available software. These instances of computer-aided instruction are perfectly natural because computers are so central to the entire field of fractal geometry. The contemporary nature of the field is revealed by a supply of mathematical problems that are simple to state but remain unsolved. Altogether, many fields of interest to non-science students have surprising examples of fractal structures. Fractal geometry is a powerful tool for imparting to non-science students some of the excitement for science often invisible to them. Several views of this are presented in Frame and Mandelbrot (2001).

The importance of fractals in the practice of science and engineering is undeniable. But fractals are also a proven force in science education. Certainly, the boundaries of fractal geometry have not yet been reached.

SEE ALSO THE FOLLOWING ARTICLES

CHAOS • PERCOLATION • TECTONOPHYSICS

BIBLIOGRAPHY

Alligood, K., and Yorke, J. (1992). *Ergodic Theory Dynam. Syst.* **12,** 377–400.
Alligood, K., Sauer, T., and Yorke, J. (1997). "Chaos. An Introduction to Dynamical Systems," Springer-Verlag, New York.
Barnsley, M. (1988). "Fractals Everywhere," 2nd ed., Academic Press, Orlando, FL.
Barnsley, M., and Demko, S. (1986). "Chaotic Dynamics and Fractals," Academic Press, Orlando, FL.
Barnsley, M., and Hurd, L. (1993). "Fractal Image Compression," Peters, Wellesley, MA.
Batty, M., and Longley, P. (1994). "Fractal Cities," Academic Press, London.
Beardon, A. (1983). "The Geometry of Discrete Groups," Springer-Verlag, New York.
Beck, C., and Schlögl, F. (1993). "Thermodynamics of Chaotic Systems: An Introduction," Cambridge University Press, Cambridge.
Berger, J., and Mandelbrot, B. (1963). *IBM J. Res. Dev.* **7,** 224–236.
Berry, M. (1979). "Structural Stability in Physics," Springer-Verlag, New York.
Bertoin, J. (1996). "Lévy Processes," Cambridge University Press, Cambridge.
Besicovitch, A., and Moran, P. (1945). *J. Lond. Math. Soc.* **20,** 110–120.
Birkhoff, G. (1927). "Dynamical Systems, American Mathematical Society, Providence, RI.
Birman, J., and Williams, R. (1983). *Topology* **22,** 47–82.
Bishop, C., and Jones, P. (1997). *Acta Math.* **179,** 1–39.
Blanchard, P. (1994). *In* "Complex Dynamical Systems. The Mathematics behind the Mandelbrot and Julia Sets" (Devaney, R., ed.), (pp. 139–154, American Mathematical Society, Providence, RI.
Bochner, S. (1955). "Harmonic Analysis and the Theory of Probability," University of California Press, Berkeley, CA.
Bowen, R. (1975). "Equilibrium States and the Ergodic Theory of Anosov Diffeomorphisms," Springer-Verlag, New York.
Bunde, A., and Havlin, S. (1991). "Fractals and Disordered Systems," Springer-Verlag, New York.
Cartwright, M., and Littlewood, L. (1945). *J. Lond. Math. Soc.* **20,** 180–189.
Cherbit, G. (1987). "Fractals. Non-integral Dimensions and Applications," Wiley, Chichester, UK.
Chorin, J. (1981). *Commun. Pure Appl. Math.* **34,** 853–866.
Crilly, A., Earnshaw, R., and Jones, H. (1991). "Fractals and Chaos," Springer-Verlag, New York.
Crilly, A., Earnshaw, R., and Jones, H. (1993). "Applications of Fractals and Chaos," Springer-Verlag, New York.
Curry, J., Garnett, L., and Sullivan, D. (1983). *Commun. Math. Phys.* **91,** 267–277.
Dekking, F. M. (1982). *Adv. Math.* **44,** 78–104.
Devaney, R. (1989). "An Introduction to Chaotic Dynamical Systems," 2nd ed., Addison-Wesley, Reading, MA.
Devaney, R. (1990). "Chaos, Fractals, and Dynamics. Computer Experiments in Mathematics," Addison-Wesley, Reading, MA.
Devaney, R. (1992). "A First Course in Chaotic Dynamical Systems. Theory and Experiment," Addison-Wesley, Reading, MA.
Devaney, R. (ed.). (1994). "Complex Dynamical Systems. The Mathematics Behind the Mandelbrot and Julia Sets," American Mathematical Society, Providence, RI.

Devaney, R., and Keen, L. (1989). "Chaos and Fractals. The Mathematics Behind the Computer Graphics," American Mathematical Society, Providence, RI.
Douady, A., and Hubbard, J. (1984). "Étude dynamique des polynômes complexes. I, II," Publications Mathematiques d'Orsay, Orsay, France.
Douady, A., and Hubbard, J. (1985). *Ann. Sci. Ecole Norm. Sup*. **18,** 287–343.
Edgar, G. (1990). "Measure, Topology, and Fractal Geometry," Springer-Verlag, New York.
Edgar, G. (1993). "Classics on Fractals," Addison-Wesley, Reading, MA.
Edgar, G. (1998). "Integral, Probability, and Fractal Measures," Springer-Verlag, New York.
Eglash, R. (1999). "African Fractals. Modern Computing and Indigenous Design," Rutgers University Press, New Brunswick, NJ.
Encarncação, J., Peitgen, H.-O., Sakas, G., and Englert, G. (1992). "Fractal Geometry and Computer Graphics," Springer-Verlag, New York.
Epstein, D. (1986). "Low-Dimensional Topology and Kleinian Groups," Cambridge University Press, Cambridge.
Evertsz, C., Peitgen, H.-O., and Voss, R. (eds.). (1996). "Fractal Geometry and Analysis. The Mandelbrot Festschrift, Curaçao 1995," World Scientific, Singapore.
Falconer, K. (1985). "The Geometry of Fractal Sets," Cambridge University Press, Cambridge.
Falconer, K. (1987). *Math. Intelligencer* **9,** 24–27.
Falconer, K. (1990). "Fractal Geometry. Mathematical Foundations and Applications," Wiley, Chichester, UK.
Falconer, K. (1997). "Techniques in Fractal Geometry," Wiley, Chichester, UK.
Family, F., and Vicsek, T. (1991). "Dynamics of Fractal Surfaces," World Scientific, Singapore.
Feder, J. (1988). "Fractals," Plenum Press, New York.
Feder, J., and Aharony, A. (1990). "Fractals in Physics. Essays in Honor of B. B. Mandelbrot," North-Holland, Amsterdam.
Fisher, Y. (1995). "Fractal Image Compression. Theory and Application," Springer-Verlag, New York.
Flake, G. (1998). "The Computational Beauty of Nature. Computer Explorations of Fractals, Chaos, Complex Systems, and Adaptation," MIT Press, Cambridge, MA.
Fleischmann, M., Tildesley, D., and Ball, R. (1990). "Fractals in the Natural Sciences," Princeton University Press, Princeton, NJ.
Frame, M., and Mandelbrot, B. (2001). "Fractals, Graphics, and Mathematics Education," Mathematical Association of America, Washington, DC.
Frostman, O. (1935). *Meddel. Lunds. Univ. Math. Sem*. **3,** 1–118.
Gazalé, M., (1990). "Gnomon. From Pharaohs to Fractals," Princeton University Press, Princeton, NJ.
Grist, R. (1997). *Topology* **36,** 423–448.
Gulick, D. (1992). "Encounters with Chaos," McGraw-Hill, New York.
Hadamard, J. (1898). *J. Mathematiques* **5,** 27–73.
Hardy, G. (1916). *Trans. Am. Math. Soc.* **17,** 322–323.
Hastings, H., and Sugihara, G. (1993). "Fractals. A User's Guide for the Natural Sciences," Oxford University Press, Oxford.
Hovi, J.-P., Aharony, A., Stauffer, D., and Mandelbrot, B. B. (1996). *Phys. Rev. Lett.* **77,** 877–880.
Hutchinson, J. E. (1981). *Ind. Univ. J. Math.* **30,** 713–747.
Keen, L. (1994). *In* "Complex Dynamical Systems. The Mathematics behind the Mandelbrot and Julia Sets" (Devaney, R., ed.), pp. 139–154, American Mathematical Society, Providence, RI.
Keen, L., and Series, C. (1993). *Topology* **32,** 719–749.
Keen, L., Maskit, B., and Series, C. (1993). *J. Reine Angew. Math.* **436,** 209–219.
Kigami, J. (1989). *Jpn. J. Appl. Math.* **8,** 259–290.
Lapidus, M. (1995). *Fractals* **3,** 725–736.
Lapidus, M., Neuberger, J., Renka, R., and Griffith, C. (1996). *Int. J. Bifurcation Chaos* **6,** 1185–1210.
Lasota, A., and Mackey, M. (1994). "Chaos, Fractals, and Noise. Stochastic Aspects of Dynamics," 2nd ed., Springer-Verlag, New York.
Lawler, G., Schramm, O., and Warner, W. (2000). *Acta Math.*, to appear [xxx.lanl.gov./abs/math. PR/0010165].
Lei, T. (2000). "The Mandelbrot Set, Theme and Variations," Cambridge University Press, Cambridge.
Le Méhauté, A. (1990). "Fractal Geometries. Theory and Applications," CRC Press, Boca Raton, FL.
Levinson, N. (1949). *Ann. Math.* **50,** 127–153.
Lorenz, E. (1963). *J. Atmos. Sci.* **20,** 130–141.
Lu, N. (1997). "Fractal Imaging," Academic Press, San Diego.
Lyubich, M. (2001). *Ann. Math.,* to appear.
Mandelbrot, B. (1975). *C. R. Acad. Sci. Paris* **280A,** 1075–1078.
Mandelbrot, B. (1975, 1984, 1989, 1995). "Les objects fractals," Flammarion, Paris.
Mandelbrot, B. (1976). *C. R. Acad. Sci. Paris* **282A,** 119–120.
Mandelbrot, B. (1980). *Ann. N. Y. Acad. Sci.* **357,** 249–259.
Mandelbrot, B. (1982). "The Fractal Geometry of Nature," Freeman, New York.
Mandelbrot, B. (1984). *J. Stat. Phys.* **34,** 895–930.
Mandelbrot, B. (1985). *In* "Chaos, Fractals, and Dynamics" (Fischer, P., and Smith, W., eds.), pp. 235–238, Marcel Dekker, New York.
Mandelbrot, B. (1995). *J. Fourier Anal. Appl.* **1995,** 409–432.
Mandelbrot, B. (1997a). "Fractals and Scaling in Finance. Discontinuity, Concentration, Risk," Springer-Verlag, New York.
Mandelbrot, B. (1997b). "Fractales, Hasard et Finance," Flammarion, Paris.
Mandelbrot, B. (1999). "Multifractals and $1/f$ Noise. Wild Self-Affinity in Physics," Springer-Verlag, New York.
Mandelbrot, B. (2001a). *Quant. Finance* **1,** 113–123, 124–130.
Mandelbrot, B. (2001b). "Gaussian Self-Affinity and Fractals: Globality, the Earth, $1/f$ Noise, & R/S," Springer-Verlag, New York.
Mandelbrot, B. (2001c). "Fractals and Chaos and Statistical Physics," Springer-Verlag, New York.
Mandelbrot, B. (2001d). "Fractals Tools," Springer-Verlag, New York.
Mandelbrot, B. B., and Stauffer, D. (1994). *J. Phys. A* **27,** L237–L242.
Mandelbrot, B. B., Vespignani, A., and Kaufman, H. (1995). *Europhy. Lett.* **32,** 199–204.
Maksit, B. (1988). "Kleinian Groups," Springer-Verlag, New York.
Massopust, P. (1994). "Fractal Functions, Fractal Surfaces, and Wavelets," Academic Press, San Diego, CA.
Mattila, P. (1995). "Geometry of Sets and Measures in Euclidean Space. Fractals and Rectifiability," Cambridge University Press, Cambridge.
McCauley, J. (1993). "Chaos, Dynamics and Fractals. An Algorithmic Approach to Deterministic Chaos," Cambridge University Press, Cambridge.
McLaughlin, J. (1987). *Proc. Am. Math. Soc.* **100,** 183–186.
McMullen, C. (1994). "Complex Dynamics and Renormalization," Princeton University Press, Princeton, NJ.
McShane, G., Parker, J., and Redfern, I. (1994). *Exp. Math.* **3,** 153–170.
Meakin, P. (1996). "Fractals, Scaling and Growth Far from Equilibrium," Cambridge University Press, Cambridge.
Milnor, J. (1989). *In* "Computers in Geometry and Topology" (Tangora, M., ed.), pp. 211–257, Marcel Dekker, New York.
Moon, F. (1984). *Phys. Rev. Lett.* **53,** 962–964.
Moon, F. (1992). "Chaotic and Fractal Dynamics. An Introduction for Applied Scientists and Engineers," Wiley-Interscience, New York.
Parker, J. (1995). *Topology* **34,** 489–496.
Peak, D., and Frame, M. (1994). "Chaos Under Control. The Art and Science of Complexity," Freeman, New York.
Peitgen, H.-O. (1989). "Newton's Method and Dynamical Systems," Kluwer, Dordrecht.

Peitgen, H.-O., and Richter, P. H. (1986). "The Beauty of Fractals," Springer-Verlag, New York.
Peitgen, H.-O., and Saupe, D. (1988). "The Science of Fractal Images," Plenum Press, New York.
Peitgen, H.-O., Jürgens, H., and Saupe, D. (1992). "Chaos and Fractals: New Frontiers of Science," Springer-Verlag, New York.
Peitgen, H.-O., Rodenhausen, A., and Skordev, G. (1998). *Fractals* **6,** 371–394.
Pietronero, L. (1989). "Fractals Physical Origins and Properties," North-Holland, Amsterdam.
Pietronero, L., and Tosatti, E. (1986). "Fractals in Physics," North-Holland, Amsterdam.
Poincaré, H. (1890). *Acta Math.* **13,** 1–271.
Pollard-Gott, L. (1986). *Language Style* **18,** 233–249.
Rogers, C. (1970). "Hausdorff Measures," Cambridge University Press, Cambridge.
Ruelle, D. (1978). "Thermodynamic Formalism: The Mathematical Structures of Classical Equilibrium Statistical Mechanics," Addison-Wesley, Reading, MA.
Ruelle, D., and Takens, F. (1971). *Commun. Math. Phys.* **20,** 167–192.
Samorodnitsky, G., and Taqqu, M. (1994). "Stable Non-Gaussian Random Processes. Stochastic Models with Infinite Variance," Chapman and Hall, New York.
Sapoval, B. (1989). *Physica D* **38,** 296–298.
Sapoval, B., Rosso, M., and Gouyet, J. (1985). *J. Phys. Lett.* **46,** L149–L156.
Sapoval, B., Gobron, T., and Margolina, A. (1991). *Phys. Rev. Lett.* **67**, 2974–2977.
Scholz, C., and Mandelbrot, B. (1989). "Fractals in Geophysics," Birkhäuser, Basel.
Shishikura, M. M. (1994). *Astérisque* **222,** 389–406.
Shlesinger, M., Zaslavsky, G., and Frisch, U. (1995). "Lévy Flights and Related Topics in Physics," Springer-Verlag, New York.
Sinai, Y. (1972). *Russ. Math. Surv.* **27,** 21–70.
Smale, S. (1963). *In* "Differential and Combinatorial Topology" (Cairns, S., ed.), pp. 63–80, Princeton University Press, Princeton, NJ.
Stauffer, D., and Aharony, A. (1992). "Introduction to Percolation Theory," 2nd ed., Taylor and Francis, London.
Strogatz, S. (1994). "Nonlinear Dynamics and Chaos, with Applications to Chemistry, Physics, Biology, Chemistry, and Engineering," Addison-Wesley, Reading, MA.
Sullivan, D. (1985). *Ann. Math.* **122,** 410–418.
Tan, Lei (1984). *In* "Étude dynamique des polynômes complexes" (Douardy, A., and Hubbard, J., eds.), Vol. II, pp. 139–152, Publications Mathematiques d'Orsay, Orsay, France.
Tan, Lei. (2000). "The Mandelbrot Set, Theme and Variations," Cambridge University Press, Cambridge.
Thurston, W. (1997). "Three-Dimensional Geometry and Topology," Princeton University Press, Princeton, NJ.
Tricot, C. (1982). *Math. Proc. Camb. Philos. Soc.* **91,** 54–74.
Vicsek, T. (1992). "Fractal Growth Phenomena," 2nd ed., World Scientific, Singapore.
Voss, R., and Clarke, J. (1975). *Nature* **258,** 317–318.
West, B. (1990). "Fractal Physiology and Chaos in Medicine," World Scientific, Singapore.
Weyl, H. (1912). *Math. Ann.* **71,** 441–479.
Williams, R. (1983). *Ergodic Theory Dynam. Syst.* **4,** 147–163.
Wiggins, S. (1990). "Introduction to Applied Nonlinear Dynamical Systems and Chaos," Springer-Verlag, New York.
Witten, T., and Sander, L. (1981). *Phys. Rev. Lett.* **47,** 1400–1403.
Witten, T., and Sander, L. (1983). *Phys. Rev. B* **27,** 5686–5697.